ABSTRACT

HETERGENEOUS OIL SATURATION IN SUBMARINE CHANNEL AND ADJACENT FACIES, MONTEREY FORMATION, POINT FERMIN, PALOS VERDES, CALIFORNIA

By

Nawaf S. AlShammary

May 2013

Extreme heterogeneity in oil saturation between closely adjacent sandstone beds reflects different timing and degree of diagenesis. Understanding the distribution and origin of such heterogeneity is critical to effectively exploiting intercalated sandstone deposits within fine-grained unconventional reservoirs and in unraveling subtleties of stratigraphic traps. Sea cliff exposures at Point Fermin, California, expose a submarine channel facies within the largely hemipelagic facies. Separated by only meters, Point Fermin Sandstone is oil-saturated, whereas Altamira Shale sandstone is not. Samples were analyzed for porosity, permeability and fluid saturation in conjunction with thin-section petrographic analysis. Sandstones are primarily schist- bearing lithic arenites and the grains are cemented mostly by rhombic dolomite. Data show that both units have the same provenance but differ in the timing and type of diagenesis with shale-hosted sandstones generally showing earlier cementation. The degree and type of cementation occluded pore spaces to prevent hydrocarbon charging in the non-saturated sandstone.

HETERGENEOUS OIL SATURATION IN SUBMARINE CHANNEL AND ADJACENT FACIES, MONTEREY FORMATION, POINT FERMIN, PALOS VERDES, CALIFORNIA

A THESIS

Presented to the Department of Geological Sciences

California State University, Long Beach

In Partial Fulfillment

of the Requirements for the Degree

Master of Science in Geology

By Nawaf S. AlShammary

B.S., 2000, University of New Orleans

May 2013

WE, THE UNDERSIGNED MEMBERS OF THE COMMITTEE,

HAVE APPROVED THIS THESIS

HETERGENEOUS OIL SATURATION IN SUBMARINE CHANNEL AND ADJACENT FACIES, MONTEREY FORMATION, POINT FERMIN, PALOS VERDES, CALIFORNIA

By

Nawaf S. AlShammary

COMMITTEE MEMBERS

Richard J. Behl, Ph.D. (Chair)	Geological Sciences
Donald D. Clarke	Consulting Geologist
Thomas Kelty, Ph.D.	Geological Sciences

ACCEPTED AND APPROVED ON BEHALF OF THE UNIVERSITY

Robert D. Francis, Ph.D.
Department Chair, Department of Geological Sciences

California State University, Long Beach

May 2013

ACKNOWLEDGMENTS

I would like to sincerely thank Dr. Rick Behl for giving me the chance to be his student. I appreciate that on top of the busy schedule and illness, he got this thesis going. I appreciate your guidance and professionalism. You are my science hero.

I must thank Don Clarke for his amazing kindness and support in my research. I am greatly in debt for your support. Thank you to Dr. Tom Kelty for his support and being in my thesis committee. I appreciate my thesis committee members for being extremely supportive for me in this research. Thanks for Chuck Herzig for his help and his petrographical insight. Thanks for Dr. Greg Holk for accepting me in this amazing school and city. I never felt a stranger here.

Thank you for my family for supporting me in my pursuit of a master's degree. Thank you to my father Slobi, all my hard work is for you. Thank you to my mother Tamsha, I hope to be your best son. Thank you to my grandmother Adela, who taught me the meaning of love.

Thank you to my wife Norah, my unconditional love, who supported me in the good and bad days. Thank you to my son and best friend Mohammed, keep up your love for science and knowledge. Thank you for my daughter Khayal, my little angel. Thank you for my son Nemer, my little teddy bear.

Thank you to my brothers Abdullah, Abdulrahman, and Abdulrazaq, thank you for your support. Thank you for my sisters Alia, Ghalia, Dalal, and Nawal, you all are

very close to my heart. Thanks for my MARS project teammates Opral, Heather, Kassa, Becca, and the rest for their support and the great team we had.

Thanks to Talal AlKhashrami my previous division head for his support and encouragements. Thank you to Norma Yanni, my Aramco academic advisor for her amazing support during my master's program. Thanks to Nelson Robinson for his support in this master's program. Thanks to Roy Burnstad, my old officemate for the encouragements and his friendship. Thanks to Najwa AlAzimi for her support on my master's program. Thanks to Abdulfattah Bakhit for encouraging me to make the switch to geology. Thank you to Aramco management and co-workers who made this possible.

TABLE OF CONTENTS

Page

CHAPTER Page

LIST OF TABLES

LIST OF FIGURES

FIGURE Page

FIGURE Page

FIGURE Page

CHAPTER 1

INTRODUCTION

The nature and challenge of hydrocarbon exploration and production is changing in a fundamental way. In the past century, large and relatively easy to find structural traps were the main target of exploration. As those giants are depleted, more subtle stratigraphic traps and unconventional reservoirs are becoming the new targets for exploration. The U.S. Department of Energy outlook report for 2013 shows this important shift in exploration towards unconventional reservoirs in their forecast to 2040 (U.S. Energy Information Administration, 2013). They predict that as soon as 2020, about one third of U.S. oil production will come from low-permeability "tight" oil reservoirs. As the petroleum industry transitions from conventional clastic and carbonate reservoirs to unconventional reservoirs, understanding how and why porosity and permeability varies is increasingly important. Effective exploitation of stratigraphic and unconventional reservoirs requires understanding all aspects of the geology of the explored area including sedimentology, stratigraphy and diagenesis.

The depositional and diagenetic environment plays a key role in defining stratigraphic traps and unconventional reservoirs. Diagenetic changes that affect adjacent units of sedimentary rocks might be the difference between a reservoir and a non-reservoir. It is now appreciated that there is greater variability in depositional environment and sedimentology in fine-grained deposits than previously understood. As

we enter the 21st century, we have more knowledge about new concepts in geology and especially fine grained sediments (Bramlette, 1946; Passey et al., 2012; Basinski, 2013). Volumetrically minor sandstone beds in otherwise fine-grained rocks can play important roles in exploiting unconventional reservoirs, as both zones of storage and in providing connectivity between the overall fine-grained matrix and the well bore. For example, even a submarine slope deposit the minor sandstone surrounded by slope shales can form a good stratigraphic trap (Slatt, 1986; Hewlett and Jordan, 1994).

Because of these reasons, it is critical to locate areas where the physical properties of sandstone in sand-poor unconventional reservoirs can be studied and observed lateral and vertical variability can be investigated and explained. One excellent site for such a study is at Point Fermin, California, where the fine-grained, organic-rich Monterey Formation contains intercalated sandstone beds and lenses and is cut by a distinct submarine channel deposit (FIGURE 1). This exposure provides the opportunity to study remarkable variations in porosity and hydrocarbon saturation over short distances that are related to original differences in depositional and diagenetic environment within a primarily hemipelagic setting.

The Miocene Monterey Formation has long been studied, in part because of its role as both a major source and fractured reservoir of petroleum in California (Bramlette, 1946; Pisciotto and Garrison, 1981; Isaacs, 1980; Behl, 1999). With the exception of the highly prolific Stevens Sand of the San Joaquin Basin (Harrison and Graham, 1999), coarse clastics have been little studied in the Monterey, with most studies being of the hemipelagic, fine-grained, and siliceous or calcareous lithofacies.

FIGURE 1. Point Fermin, San Pedro, Palos Verdes Peninsula.

The outcrops in the sea cliffs at Point Fermin provide an extraordinary opportunity to investigate the different potential controls of sandstone porosity and oil saturation in two adjacent units—the Altamira Shale and Point Fermin Sandstone. The Altamira Shale Member of the Monterey Formation (Woodring et al., 1946; Conrad and Ehlig, 1983) is primarily a thin-bedded organic-rich, siliceous, and variably phosphatic, dolomitic, or tuffaceous mudrock with interstratified sandstone beds and lenses. In contrast, the Point Fermin Sandstone Member of the Monterey Formation is chiefly a medium to thick bedded sandstone and conglomerate with minor intercalated shale and dolostone that was deposited as submarine channel deposits (Woodring et al., 1946; Russell, 1987). The boundary between the two units is easily traced by an intraformational breccia on the bottom of the submarine channel and the difference in bed thickness between the two units (FIGURE 2). In outcrop, there appears to be a marked heterogeneity in oil saturation between sandstones in the two adjacent units. The purpose

of this study is to: (a) understand the lateral and vertical heterogeneity in hydrocarbon saturation in the closely associated sandstones at Point Fermin, (b) compare the petrology of sandstone samples from the Point Fermin Sandstone and the adjacent Altamira Shale facies, (c) examine and explain porosity and permeability differences between the two units, and (d) to create a map to show the stratigraphic architecture.

FIGURE 2. Contact between Point Fermin Sandstone and Altamira Shale.

This study tests competing potential hypotheses to explain this observed difference in oil saturation. The first hypothesis is that porosity and permeability, and hence oil saturation, is primarily controlled by depositional environment and processes in the two adjacent facies that created sandstones with distinct primary differences in grain size, sorting. The second hypothesis is that sandstones in the two facies have

provenances significantly different enough to provide framework grains of distinct composition and diagenetic potential, thus influencing the type and timing of diagenesis and interstitial cement. The third hypothesis is that the geochemistry of the burial environment of the two facies alone, independent of texture or grain size of the framework grains, was sufficient to control different diagenetic pathways that impeded or permitted differential oil saturation.

CHAPTER 2

BACKGROUND

Geologic History and Setting of the Los Angeles Basin

The Los Angeles basin formed during the late Cenozoic in part of the former western North American forearc basin (Wright, 1991; Crouch and Suppe, 1993; Rumelhart and Ingersoll, 1997). Tectonic reorganization of the western part of the North American plate in association with the transition from a convergent to transform plate boundary, formed many relatively small sedimentary basins (Atwater, 1970; Blake et al., 1978). The LA basin formed by localized and rapid extension. Basement rocks include metamorphic core complexes exposed by detachment faults (Crouch and Suppe, 1993) or Mesozoic to lower Cenozoic sedimentary deposits (Wright, 1991; Blake, 1991). From the Miocene to Present, the Los Angeles basin evolution went through three stages: first was a transrotation (18-12 Ma), the second is transtension (12-6 Ma), and the third is transpression (6-0 Ma) (Rumelhart and Ingersoll, 1997; Ingersoll, 1999). The Los Angeles basin was probably a silled basin during the upper Miocene that intersected the oxygen-minimum oceanographic zone (Redin, 1991). The main pathways of sediment distribution for basin-filling were three submarine fans during middle to upper Miocene, Pliocene, and Pleistocene. The Tarzana fan, the San Gabriel fan, and the Santa Ana fan (Redin, 1991). These submarine fans were formed within the space opened by extension

and rotation of the western Transverse Ranges, a large crustal block that has rotated more than 90° clockwise (Crouch & Suppe, 1993).

According to Schwartz and Colburn (1987), the Los Angeles basin and Palos Verdes area developed within the context of a sequence of tectonic events. From the Mesozoic to the early Miocene, oblique subduction occurred along the western margin of the North American plate. From Oligocene to early Miocene, there was subduction of the Pacific-Farallon spreading ridge. In the early Miocene (17.5 Ma), the Los Angeles basin rapidly subsided with the onset of rifting. At 16 Ma, initialization of wrench motion and initialization of the Newport-Inglewood fault. This was followed by volcanism in Palos Verdes at 15.5 Ma. At 13.5-12 Ma, the Catalina schist become exposed which is the source terrane for the breccia and the sandstone at Point Fermin. The Los Angeles basin went through another deepening phase at 12 Ma. Northward extension of the Los Angeles basin ended at 9.5 Ma. At 5.5 Ma further deepening of Los Angeles basin and the movement slowed on the Newport-Inglewood fault, but reactivated by 3 Ma. The Los Angeles basin stopped deepening at 1.5 Ma. From 1.5 Ma to present, a reactivation of the Palos Verdes fault uplift with a reverse component created local uplift. At present there is a continued active movement of Newport-Inglewood creating uplift associated with many of the major oil fields in the Los Angeles basin. FIGURE 3 shows some of the major tectonic events time in relation to Los Angeles basin.

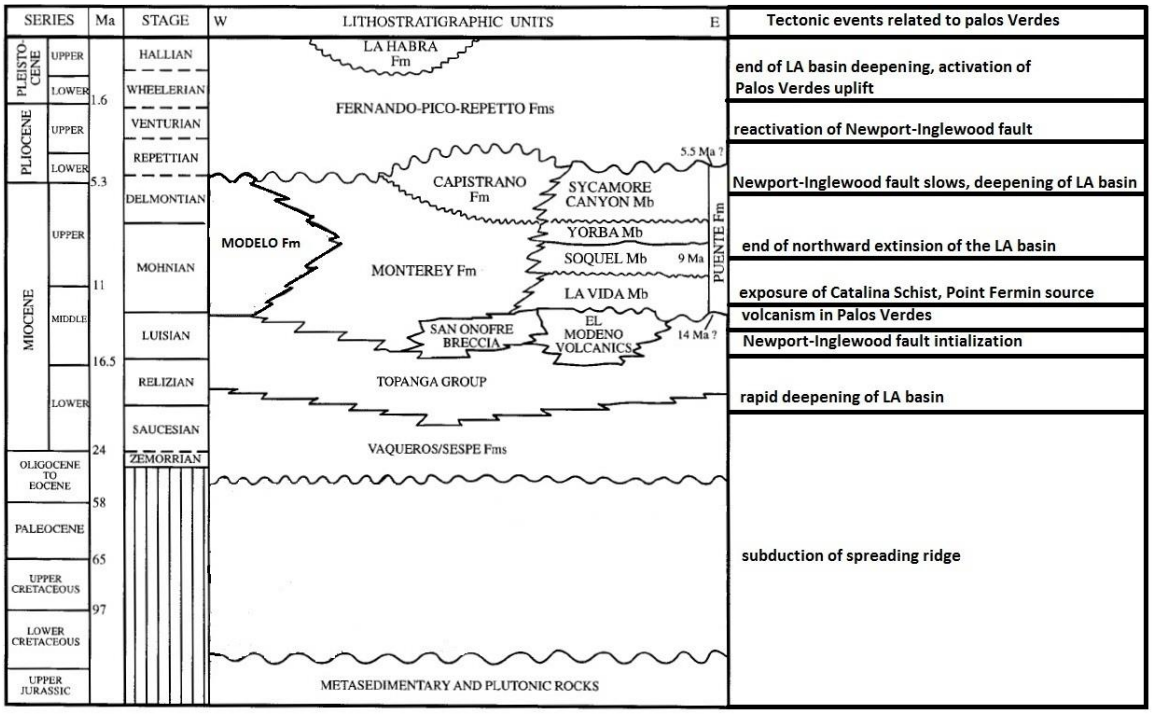

FIGURE 3. Miocene Los Angeles (LA) stratigraphy—modified from Rumelhart and Ingersoll (1997), Blake (1991), and Schwartz and Colburn (1987).

The faults within the Los Angeles basin are mainly NW-striking caused by the deformation and rotation movement between the Pacific plate and the North American plate (Luyendyk, 1991). These include: Newport-Inglewood fault, Palos Verdes fault, Elsinore fault, San Jacinto fault, Hosgri fault, East Santa Cruz Basin fault, and San Andreas fault. In Palos Verdes, which is a doubly plunging anticlinorium, there are two main faults: Palos Verdes fault and Cabrillo fault. The Palos Verdes fault is a northwest striking fault, and considered in the offshore as an active strike-slip fault (Schwiebert & Francis, 2007). The Cabrillo fault is the other major fault in Palos Verdes, measuring 16-18 km long with NE dip. The fault dies out or merges with the Palos Verdes fault (Schwiebert and Francis, 2007). In addition to the main two faults, there are other minor faults near Point Fermin and other place in Palos Verdes (Brown, 2007). The Palos

Verdes fault and the Cabrillo fault both caused the uplift of the Palos Verdes Peninsula that has started in the Late Pliocene and still active (Bryant, 1982; Ehlig, 1982).

Oil in Los Angeles Basin

The Los Angeles basin is an active oil producing area. Compared to its size, the Los Angeles basin is the most prolific oil producing basin in the world (Yerkes et al., 1965). Up to the 1990s, more than 8 billion barrels of oil and 7.5 TCF of gas has been produced from the basin (Norton and Otott, 1996). The oldest reservoir is the fractured Mesozoic Franciscan basement and the youngest is the upper Pliocene turbidite Pico Formation (Norton and Otott, 1996). Most of the oil produced in Los Angeles basin comes from channelized sand or suprafan sands of late Mohnian to Repettian age (Redin, 1991). These provide an enormous thickness of potential reservoir rocks and the majority of the oil fields in Los Angeles basin have stacked Miocene and Pliocene sand reservoirs. The two largest oil fields in Los Angeles basin are the Wilmington and the Huntington Beach oil fields (Norton and Otott, 1996). The two fields are 8 km and around 20 km to the south and east of the study area at Point Fermin. They are bounded by two northwest trending faults, the THUMS-Huntington Beach fault that joins the Palos Verdes fault to the south and the Newport-Inglewood fault to the north. Wilmington oil field is the largest producing field in Los Angeles basin, and is 19 km long by 5.3 km wide. There are six different production zones in the field starting from middle Miocene Topanga to lower Pliocene Repetto Formations. The Monterey Formation overlies the basement rocks and is correlated to Altamira Shale in Palos Verdes and its thickness is 2,500 feet (Norton and Otott, 1996; Truex, 1972). All the zones in Wilmington field are all deep-water sand turbidites from northern and eastern sources in a rapidly deepening Los

Angeles basin (Norton and Otott, 1996). The Wilmington oil field lies in a 35 km northwest trending, highly faulted, asymmetrical anticline (Clarke, 1987).

The lower part of the upper Miocene sediments in the Wilmington field has near optimal conditions for oil generation (Turcotte and McAdoo, 1979). The thermal subsidence of this part of the Los Angeles basin started with cessation of volcanism at approximately 11 Ma. This subsidence and the organic richness of portions of the Monterey or Puente sediments contributed to the oil potential of the basin. Maturity estimates show that the upper Miocene rocks are the source of hydrocarbon in the Los Angeles basin (Alan et al., 1991).

Almost all of the major oil fields in Los Angeles basin are northeast of the Palos Verdes fault, many along the Newport-Inglewood fault trend. However, oil saturated sandstone is observed at Point Fermin, located southwest of the fault, and no major oil field has been discovered southwest of the fault. Beta field is on the southwest of the fault but it is smaller in size than Wilmington and Huntington Beach fields. I think this is due to the fact that southeast of the Newport-Inglewood fault is mainly offshore. Permission for offshore drilling is not easy in the state of California due to environmental concerns.

Stratigraphy of the Monterey Formation in the Palos Verdes Hills

From the Coast Ranges of central and northern California to the inland San Joaquin Valley, the Monterey Formation can be generally subdivided into three main lithofacies (Pisciotto and Garrison, 1981). From bottom to top: 1- Lower calcareous facies, principally consisting of foraminiferal-coccolith mudstone and shale, 2- Middle transitional unit of phosphatic shale and mudstone cyclically interbedded with siliceous

rocks near its top, 3- Upper siliceous facies that includes chert, porcelanite, siliceous shale and diatomaceous strata (Pisciotto and Garrison, 1981). These large stratigraphic divisions have not been identified in the Los Angeles Basin, perhaps because the sand-rich proximal setting was unable to record the broad climatic-oceanographic changes better represented in the more-distal, finer-grained settings. Furthermore, large lateral differences in sediment character led to naming of several different co-eval formations (Monterey, Modelo, Puente, Topanga) in various locations across and surrounding the Los Angeles Basin (Blake, 1991).

The Monterey Formation in Palos Verdes was initially referred to as the Monterey Shale by Woodring et al. (1946) who measured it to be around 600 m thick and subdivided it into three members. In ascending order, these are: Altamira Shale, Valmonte Diatomite and Malaga Mudstone. The Altamira Shale started deposition around 15.5 Ma, Valmonte Diatomite beginning around 9.5 Ma, while the Malaga Mudstone was deposited around 3.5 Ma (Behl and Morita, 2007; Barron and Isaacs, 2001; Obradovich and Naeser, 1981; Conrad and Ehlig, 1983; Blake, 1991). The maximum thickness of those members is respectively 300 m, 125 m and 125 m (Conrad and Ehlig, 1983), however they vary considerably with location due to an irregular depositional topography, syn and post sedimentary mass movements, and Quaternary deformation and erosion (Conrad and Ehlig, 1983; Behl and Morita, 2007). The Altamira Shale, which is the thickest member, was subdivided to three parts: lower silty shale, middle cherty shale and upper phosphatic shale. The boundary between the middle and upper Altamira Shale corresponds to the boundary between middle and upper Miocene (Woodring et al., 1946). Conrad and Ehlig (1983) argue that the boundary between the

lower and middle Altamira Shale is impossible to map because of the gradual nature of change between the two parts. Therefore, they redivided the Altamira shale into tuffaceous, cherty and phosphatic lithofacies (oldest to youngest). Dibblee (1999) subdivided the Altamira Shale into just a lower and upper part.

Altamira Shale and Point Fermin Members

The Altamira Shale member is named after the stratigraphic section exposed in and near Altamira Canyon, which has a thickness of about 300 m. The Altamira Shale overlaps schist basement rocks north of the hills and basalt penetrates its lower and middle parts. The lower silty shale part is well exposed at Portuguese Canyon, with an exposed thickness of around 85 m, consisting mainly of silty, sandy, and siliceous shale and porcelanite (Woodring et al., 1946). Conrad (1983) combined most of Woodring et al.'s middle part with the lower part, naming it the Tuffaceous lithofacies because of intercalated volcanic ash beds. It is difficult to correlate the Tuffaceous lithofacies in the different areas of Palos Verdes, possibly indicating large variations in the original depositional bathymetry (Conrad and Ehlig, 1983). The Tuffaceous lithofacies of the Altamira Shale is the thickest and the most widely distributed of the Monterey Formation in Palos Verdes, with a thickness of around 275 m, overlapping the schist basement on the north slopes of the Portuguese Canyon (FIGURE 4) (Woodring et al., 1946; Conrad and Ehlig, 1983; Behl and Morita, 2007).The most recognizable lithology in the upper portion of the middle Altamira Shale is the Cherty lithofacies (terminology of Conrad and Ehlig, 1983) that contains thinly interbedded porcelanite, cherty porcelanite and siliceous shale with a distinctive zone of ellipsoidal opal-CT concretions (i.e., chert spheroids, see Behl, 2011) in the western half of the hills. This unit is stratigraphically equivalent with

some of the diatomaceous rocks that occur in the upper part of the Altamira Shale and overlying Valmonte Diatomite, increasing found on the east and north portions of the Palos Verdes Hills (Woodring et al., 1946). Woodring et al. (1946) did not clearly define the boundary between the middle upper members of the Altamira Shale, but described the upper member in the eastern side of Point Fermin sea cliff as consisting of porcelaneous shale, phosphatic shale, and limestone (dolostone). This upper part was named by Conrad (1983) and Conrad and Ehlig (1983) as the Phosphatic lithofacies. Dibblee (1999) combined the cherty lithofacies and the phosphatic lithofacies as the upper part in the Altamira Shale.

The Point Fermin Sandstone forms a distinctive, wave-resistant headland and the southernmost tip of the Palos Verdes Peninsula. Point Fermin was named by Vancouver during his 1793 voyage in honor of Fermin de Lausen, head of the Franciscan missions in California (Woodring et al., 1946). Woodring et al. (1946) estimated the thickness of Point Fermin Sandstone about 90 m. They noted that the blue-schist sandstone bodies thin to the east of the sea cliff. They interpreted the base of the sandstone in Point Fermin as stratigraphically equivalent to the upper part of the Altamira Shale.

Conrad and Ehlig (1983) proposed that the Point Fermin Sandstone spans the stratigraphic positions of the Cherty and Phosphatic lithofacies (middle to upper Altamira Shale) and the lower part of the Valmonte Diatomite. The lower Point Fermin Sandstone unit is composed of amalgamated, thick-bedded sandstone, breccia, conglomerate and lenses of intraformational breccia (Russell, 1987). Some beds contain rip-up clasts of the Catalina Schist up to one meter long (Conrad and Ehlig, 1983).

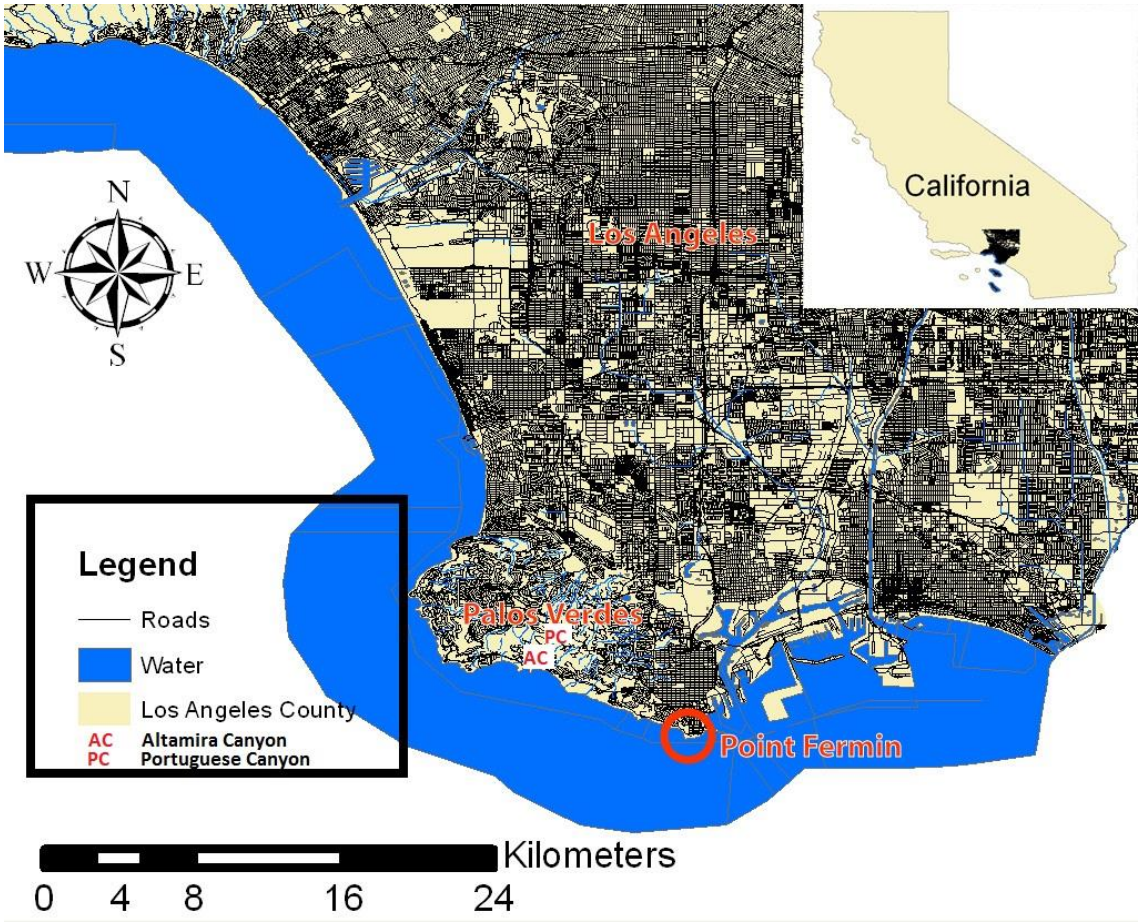

FIGURE 4. Palos Verdes and Point Fermin map.

Russell (1987) observed that the southern part of the Point Fermin Sandstone has a random, very thin to thick bedded sandstone that is often amalgamated. The sandstone of Point Fermin represents a submarine channel complex that has different channel fill episodes (Russell, 1987).

Previous Studies of the Point Fermin Sandstone

In addition to general studies of the Palos Verdes Hills (Woodring et al., 1946) or of the Monterey Formation on the peninsula (Conrad and Ehlig, 1983; Behl and Morita, 2007), there have been several studies that concentrated on the Point Fermin Sandstone.

Spotts (1964) focused on imbricated clasts and sedimentary structures to identify the paleocurrent direction in the submarine channel. In another study, Spotts and Silverman (1966) concluded that dolomite at Point Fermin was of organic origin. Sloan (1987) used radiolarians in the siltstone and claystone at Point Fermin to determine that the deposits were deposited between 12.7-11.4 Ma. He also concluded from the cold-water radiolarians that there was a strong, southward current during fan deposition. However, in a personal communication (2012) to Dr. Behl, he did not express full confidence in the robustness of the age determination. Cherven and Russell (1987) published a limited petrological study of six sandstone samples from the submarine channel deposits at Point Fermin and compared them with one sample from Beta field that they considered coeval with the Point Fermin submarine channel deposits. This study did not include analysis of the associated hemipelagic Altamira Shale deposits. In 1987, Russell published a stratigraphic and sedimentologic study on the submarine deposits that also placed little emphasis on the Altamira Shale deposits, which was slightly expanded in his 1988 Master's thesis. Spotts (1964) and Russell (1987) agreed that the source of the Point Fermin submarine channel deposits was the Catalina Schist.

Sediment Source and Transport Direction for Point Fermin Sandstone

Different paleocurrent determinations and interpretations of location of the sediment source of the submarine channel deposits of the Point Fermin Sandstone were made by previous researchers (Spotts, 1964; Conrad and Ehlig, 1983; Russell, 1987; Dibblee, 2000). One study used grain orientation and sedimentary structures to conclude the direction of the deposition, which concluded that the source of sedimentation is southeast and that the flow was to the northwest (Spotts, 1964). Dibblee (2000) reiterated

the same source direction of Spotts (1964) but provided no additional data in support. Conrad and Ehlig (1983) concluded that the source direction was to the east, but likewise provided no evidence for this direction. Finally, Russell (1987) interpreted a totally different direction using sedimentary structures that the source was to the north while the flow was to the south. Based on my own observations, it is more likely that a southeastern to eastern source provided sediment to Point Fermin because of the architecture of the submarine channel deposits and the unconformity between the Altamira Shale and Point Fermin.

Age of the Monterey Formation in Palos Verdes

The Monterey Formation (including the Altamira Shale, Valmonte Diatomite, and Malaga Mudstone) in Palos Verdes was deposited between 15 Ma-4 Ma based on radiometric dating of correlative deposits with foraminiferal assemblages characteristic of the Relizian, Luisian, Mohnian and Delmontian (Obradovitch and Naeser, 1981). Rowell (1982) dates the Monterey Formation at Palos Verdes to be 15.5-3.5 Ma. Upper Relizian benthic foraminifera collected from the lower part of the Altamira Shale correlates with the Gould Shale of the Monterey Formation in the western San Joaquin Valley (Woodring et al., 1946). The middle part of the Altamira Shale is assigned to the Luisian benthic foraminiferal stage. The Altamira Shale spans 6 million years from 15.5-9.5 Ma (Behl and Morita, 2007; Barron and Isaacs, 2001; Obradovich and Naeser, 1981; Conrad and Ehlig, 1983; Blake, 1991). The potential age range of the Point Fermin Sandstone is 14.5-10 Ma (Conrad and Ehlig, 1983).

Basement Rock of the Palos Verdes Hills

The basement rock of the Palos Verdes Peninsula is composed of metamorphic schist and altered igneous rocks. The Monterey Formation lies unconformably on the Catalina Schist (Woodring et al., 1946). There is 3 km of vertical displacement of the basement rocks from Palos Verdes to the Wilmington field across the Palos Verdes fault (Norton and Otott, 1996; Clarke, 1987).

The most common rock types are quartz-sericite schist, quartz-talc schist, and quartz-glaucophane schist (Woodring et al., 1946). More recent studies indicate that the Cretaceous Catalina Schist is composed of three facies in Palos Verdes Hills: greenschist, epidote-blueschist and possible epidote-amphibolite (Holk and Brown, 2007). The mineralogy of the schist in general is chlorite, quartz, albite, muscovite, crossite, lawsonite, epidote, glaucophane, and actinolite (Yerkes et al., 1965; Mayuga, 1970). To be more specific, the epidote-blueschist has the following mineralogy: quartz, glaucophane, and epidote; the greenschist mineralogy consists of: quartz, white mica, feldspar, chlorite, epidote, and actinolite (Holk and Brown, 2007). The metamorphic temperatures and pressures for the epidote-blueschist ($P > 9$ kb, $400°C < T < 500°C$; Evans, 1990), greenschist (2 kb $< P < 9$ kb, $400°C < T < 500°C$; Frey et al., 1991) and the possible epidote-amphibolite ($P > 6$ kb, $500°C < T < 600°C$; Frey et al., 1991). This indicates that the source rocks for the Point Fermin buried deeply to condition of around 9 kb and temperatures of around 500 °C before being uplifted and exposed to supply Point Fermin with sediments. The limited outcrop of the Catalina Schist in Palos Verdes does not include the epidote-amphibolite facies, however, Holk and Brown (2007) inferred that metamorphism reached this facies.

The sub aerial exposure of Catalina Schist is limited to two localities: the relatively small exposure in the Palos Verdes Hills and a larger expanse on Santa Catalina Island, with sea-floor locations known from limited submarine sampling (Crouch and Suppe, 1993). There is a clear lithologic and structural similarity between the Palos Verdes schists and the Catalina Island schists (Holk and Brown, 2007). Three rock units on Catalina Island are described by Platt (1975) as blueschist, green-glaucophanic greenschist and amphibolite-ultramafic rock. There is general decrease in age and degree of metamorphism westward on the island (Platt, 1975). The metamorphism of the Catalina Schist is due to high pressure-low temperature subduction, and the age for the Catalina Schist is (120-115 Ma) (Grove and Bebout, 1995).

Sandstone Diagenesis

Unconsolidated sands and lithified sandstones form many of the best petroleum reservoirs and groundwater aquifers due to their potentially high intergranular porosity and permeability. These properties degrade, however, with most cases of burial diagenesis during which porosity is decreased by compaction and diagenesis. Subsurface reservoir potential of a sandstone body is therefore dependent on the primary composition, depositional facies and resulting texture (sorting and gran size) and postdepositional diagenesis (Morad et al., 2010). The latter is controlled by the diagenetic potential of the framework grains, the geochemical environment and the burial history of the rock (Morad et al., 2010).

Aside from grain composition (e.g., arkose, quartz arenite, etc.) sandstone can be classified based on its interstitial material, principally argillaceous versus crystalline cements such as silica, dolomite, calcite and anhydrite (Waldschmidt, 1941).

Intergranular porosity is not related to mean grain size, (Smith, 1969) but is related to sorting, with better sorted sands of any grain size having greater porosity than poorly sorted sands.

Diagenesis is the changes that happen on the sediments after their deposition. Compaction and pressure dissolution are two important diagenetic processes that depend on the depth of the sediments (Tucker, 2001). Bioturbation, compaction, cementation, secondary clay mineral precipitation, and development of secondary porosity are all effects of diagenesis. There can be a complex interrelationship between steps of diagenesis (or paragenenesis). For example, with greater burial and higher temperature, the solubility of silica increases, while the solubility of carbonate and anhydrite decreases (Levandowski et al., 1973).

Dolomite Cementation

Previous work at Point Fermin found dolomite cements to be important (Spotts and Silverman, 1966), and this observation is supported by this thesis research. There are a variety of environments and processes by which dolomites are thought to form. Some of these are restricted to shallow-water mixing-zone settings, and some occur on supratidal carbonate salt-flats, and some occur on buried continental margins where large volumes of high-Mg, hypersaline brines flushed through originally calcareous deposits. None of these appear to be pertinent to the deep-water setting of the Monterey Formation. Dolomites can also form in deep-water, organic-rich sediments by a couple of proposed mechanisms-including authigenic precipitation of dolomite into pore spaces and replacement of originally calcareous sediment.

The dolomite cement in Point Fermin has been noted to be of organic origin and are crystalized in rhombohedral shape because of the oxidization of hydrocarbon (Spotts and Silverman, 1966). Methane rich fluid flow can also cause the formation of dolomite because SO_4 is reduced by methane oxidation under anaerobic conditions and precipitates dolomite (Clari et al., 2009). Spheroidal dolomite is another morphology that has a relation with oil seepage and hydrocarbon nuclei and it can be indicator of reservoir in the subsurface; the gas bubbles might have promoted bacterial activity that aided such precipitation by oxidization of hydrocarbons (Gunatilaka, 1989). Different authors have connected the spheroidal dolomite cement to bacterial activities (Nielson et al., 1997; Cavagna et al., 1999; Gunatilaka, 1989).

Dolomite diagenesis happens at shallow depths from few centimeters to hundreds of meters (Shimmield and Price, 1984; Suess et al., 1988; Wefer et al., 1998; Fayek et al., 2001). The environment of dolomite formation is characterized by sulfate reduction, high alkalinity, and a rate of deposition that preserves organic carbon below the sediment/water interface (Wefer et al., 1998; Mazzullo, 2000; Wright and Wacey, 2005; Marfil et al., 2010; Baker and Burns, 1985; Baker and Kastner, 1981; Compton, 1988; Kastner et al., 1990). Many dolomites are associated with sulfate reduction and methanogenesis and those processes are carried by bacteria (Mazzullo, 2000). These types of dolomite are called organogenic dolomite. The sulfate reduction zone is shallower than the methanogenesis and the two are mutually exclusive processes. Sulfate-reduction dolomites are generally Fe-deficient while the methanogenetic are more ferroan (Mazzullo, 2000).

Wefer et al. (1998) observed the presence of dolomite and phosphate which are stimulated by the high organic productivity. They also observed a mutual exclusive relation between the dolomite crystals and the calcite which indicated a chemical setting preferable for the dolomite formation. Also there is no relation between the dolomite layers and the dolomite rhombs that can be found as cement (Wefer et al., 1998). Disseminated dolomite is found in turbidite deposits and submarine channels associated with turbidites (Marfil et al., 2010; Wafer et al., 1998) Calcite might form first in skeletal voids (Marfil et al., 2010).

Wright and Wacey (2005) managed to precipitate dolomite in culture experiments that simulated microbiogeochemical conditions found in dolomite producing lakes. Within two months, they confirmed the production of sub-spherical, sub-micron-size dolomite crystals. This gives empirical proof that bacterial sulfate reduction drives the formation of dolomite.

CHAPTER 3

METHODS

Mapping

I used two methods to map the sea cliff at Point Fermin. Because the focus of the study is the sandstone and its differences between the Altamira Shale and Point Fermin units, I focused primarily on the distribution of the sandstone beds. Sandstone beds were mapped manually in the Altamira Shale unit due to the limited extent and thickness of the beds, Sandstone beds were mapped on a panoramic image of the whole sea cliff composed of a composite of 22 photographic images. LiDAR (Laser Imaging Detection and Ranging) was shot on the sea cliff to try to measure and map the sandstone beds, but this technique did not give good results.

Sandstone deposits in the Altamira Shale ranged from medium-thick beds to laminations too small to map. I used the criteria for mapping in the Altamira Shale that the sandstone bed thickness had to be $\geq$ 10 cm. Many beds are lenticular or pinch and swell. Some beds thin to less than 10 cm and thicken to more than 20 cm and some are just isolated lenses of sandstone that up to 2 m wide. Some beds grade laterally in texture to become muddier or change to mudstone. Eleven sandstone beds in the mapped portion of the Altamira Shale unit met this criteria. A landslide covers part of the studied section of the Altamira Shale, but I was able to trace the sandstone beds across this discontinuity in the unit. The apparent dip is around 15° in general for the Altamira Shale beds. For

this hand-drawn map, the zero coordinate is the northernmost exposure of the unit at sea level. The horizontal length of the mapped Altamira Shale unit outcrop from the zero point to where the disconformable contact with the Point Fermin Sandstone reaches the base of the cliffs is 87 m. Because the nearly vertical sea cliffs are ~40 meters high, I could not reach the upper parts, but based on the apparent dip projection, a reasonable map is produced with ~ 1 m accuracy in the lower part and ~ 5 m accuracy in the upper parts.

In the Point Fermin unit, I relied mainly on photographic images to map the beds because they gave a wide view of the sea cliff making it possible to trace the thicker and more continuous sandstone beds and to record the location of samples. Photographic images were shot in a very low tide in order to get the whole height of the cliff. Twenty two images were taken to create a composite panorama of the western side of the cliff. The images were combined in Adobe Photoshop using the photomerge process. Auto option was then applied, which distorted the images to compensate for different angles or distance. The panorama was modified slightly to fix the auto merging errors. Beds on the Point Fermin sandstone were then mapped on the image in order to locate the exact positions of samples and to trace the continuity of the beds.

Conventional Core Analysis

Samples taken from the outcrop were sent to Core Laboratories. The size of the sample had to be greater than 1 in x 1 in x 2 in for "conventional core analysis." Conventional core analysis provides important data about the samples, including: porosity, permeability, fluid saturation including oil and water, grain density, sample weight, humidity report, and clay factor. These measurements are accompanied by a

white light photographic image, UV light image, and a sample description. This important information can be used to calculate other parameters including oil percentage in rock volume. The white light images show each sample under normal light, while the ultraviolet images indicate the presence of fluorescing hydrocarbons. Images were not provided for all the samples.

TABLE 1. Procedures for Conventional Core Analysis (Core Laboratories, 2012)

	Procedure (1)	Procedure (2)	Procedure (3)	Procedure (4)	Procedure (5)
Sampling Method	Arbor Cut	Drilled	Drilled	Drilled	Carved
Drill Coolant	N/A	Liquid Nitrogen	Liquid Nitrogen	Liquid Nitrogen	N/A
Jacket Material	Lead/Nickel	Lead/Nickel	None	None	None
Saturation Method	Dean Stark (Toluene)	Dean Stark (Toluene)	Dean Stark (Toluene)	Dean Stark (Toluene)	Dean Stark (Toluene)
Porosity Method					
Grain Volume	Boyle's Law (Helium)	Boyle's Law (Helium)	Boyle's Law (Helium)	Boyle's Law (Helium)	Bulk Vol-Pore Vol
Pore Volume	Boyle's Law (Helium)	Boyle's Law (Helium)	Bulk Vol-Grain Vol	Boyle's Law (Helium)	Bulk Vol-Grain Vol
Bulk Volume	Pore Vol + Grain Vol	Pore Vol + Grain Vol	Mercury Displacement	Pore Vol + Grain Vol	Mercury Displacement
Permeability Method	Air	Air	Air	Air	Emprical

Core Laboratories has 5 procedures for conventional core analysis. Procedure #4 (TABLE 1) with the following parameters was used for this study. Sampling method: drilled; drill coolant: liquid nitrogen; jacket material: none; saturation method: Dean

Stark (Toluene); grain volume: Boyle's Law (Helium); pore volume: Boyle's Law (Helium); bulk volume: pore volume + grain volume; and permeability method: air.

Conventional core analysis determined porosity and permeability with respect to air (not water or oil) under normal pressure, using helium as the experimental gas. The Dean Stark method is a measurement of fluid saturation by distillation extraction. The two fluids measured are oil and water. First, the sample is weighed. Then, the sample is heated to evaporation of water and the vapor collected to get water volume. Next, solvent is run through the sample to collect oil for at least two days. Then the post-solvent-extracted sample is weighed to give the before and after extraction difference which also allows the percentage of the fluids to be calculated. The volume of fluids that is gathered is calculated against the pore volume of the sample. In other words, it calculates the fluid percentages in the rock porosity.

Conventional core analysis laboratory used helium to determine air permeability under normal pressure to provide porosity and permeability values.

Sample Labeling

Altamira Shale samples were labeled with the abbreviation "AS" followed by a number less than 100, for example "AS-003." The Point Fermin unit samples begin with "PF" followed by a number more than 100, for example "PF-104."

Sample Size

The samples taken from the outcrop were usually fist-size. Some samples were friable and hard to obtain in one undamaged piece. Once collected, samples were cut to the appropriate size with water-cooled diamond saws in the CSU Long Beach Geology

Department. They were then shipped to commercial labs for conventional core analysis and thin section preparation.

Description

The description provided by the conventional core analysis included: rock type, color, grain size, visual porosity, and visual fluorescence. More detailed and quantitative description of porosity and composition is developed by petrographic examination of the thin sections, Porosity is subdivided into intergranular, intragranular, and fracture porosity percentages.

Grain Density and Sample Weight

The grain density of the samples is given in grams per cubic centimeter and indicates, in indirect way, the type of minerals that might be present in the sample. This data is presented in the humidity table which also includes: porosity difference, oil saturation, water saturation, and weight, under routine conditions and humid conditions. The clays will pick up excess moisture or humidity and swell. This swelling causes a difference in rock volume that is an indirect way to measure the clays, but depends on the clay type present. This test was applied to only a few samples because my samples are somewhat weathered outcrop samples, and the measurement might be not representative of original conditions. Furthermore, the clays are not an important focus of this research.

Petrographic Analysis

Petrographic analysis is the main part of this research. Thin sections of outcrop samples were prepared 1 in x 1.75 in area and polished to 30 μm thickness. Some muddy samples were made thinner. Porosity was impregnated by blue epoxy to facilitate

identification of primary features and to help distinguish them from preparation artifacts. This is accomplished by removing air from the sample under high vacuum, submerging the sample in the liquid epoxy and then pressurizing it to drive the epoxy into the porosity spaces. Mineral stains were applied to the thin sections to help in positive identification of feldspar and carbonate grains or cement. Na-cobalitinitrite stains K-feldspar yellow while Alizarin red-S will stain calcite pink and not affect dolomite. The thin sections provide us with: grain size, sorting, porosity, porosity types, compaction, cementation, cement type, mineral composition, rock classification, and other parameters or observations. Infinity software was used to take photomicrographs of the thin sections and to perform quantitative analysis. The images will be corrected on the software for light exposure to accurately show points of interest on the thin sections.

Point counting using the Gazzi-Dickinson method was applied to all sandstone thin sections. Point counting is a procedure that selects points on each thin section, removing the investigator's bias. A minimum of 300 points were determined on each thin section. These data provide information on the relative volume of each mineral on the sample. The Gazzi-Dickinson method was chosen because it maximizes the information on the source rock (provenance), minimizes the time, and minimizes variation of composition with grain size (Ingersoll et al., 1984).

QFL (Quartz-Feldspar-Lithic) provenance discrimination diagram were created to aid identification of the provenance and to determine if there are differences between the Altamira Shale and Point Fermin sandstones. To calculate the values for Q-F-L triangular diagram, the value of each Q, F, or L was divided by the total of the three, without the addition of any other value that would affect the total, such as: porosity, cement, or miscellaneous. Since

cementation plays an important role in differentiating between the Altamira Shale and Point Fermin units, another diagram will be used to show quantification of the cementation. Diagrams to show the cementation percentage for each sample will also aid in understanding the depositional processes on the different sandstones.

CHAPTER 4

DATA

Map-Cross Section

The study provides two types of data, large-scale and small-scale. The large-scale data is a cross section and outcrop observations. The small-scale data includes the conventional core analysis and the petrography of the samples. 32 outcrop samples were acquired, 9 from the Altamira Shale and 23 from Point Fermin. The location of every sample is photographed. Conventional core analysis was applied to all the 32 samples. Also, thin sections are made out of the 32 samples. Out of the nine Altamira Shale member samples, one is sandy dolomite (AS-010) while two out of the 23 Point Fermin member samples are sandy dolomite (PF-150 and PF-151)

The cross-sectional map in (CROSS SECTION 1) illustrates the sandstone beds in the lower half of Point Fermin western sea cliff with samples locations. The contact between the Altamira Shale member and the Point Fermin member follows the dipping angle of the Point Fermin sandstone bodies closely. However, the contact also is not a straight line but cuts down into the Altamira Shale member. Beds in the Point Fermin member onlap the contact with the Altamira Shale member.

CROSS SECTION 1. Point Fermin cross-sectional map with samples locations (A) northern half, (B) southern half.

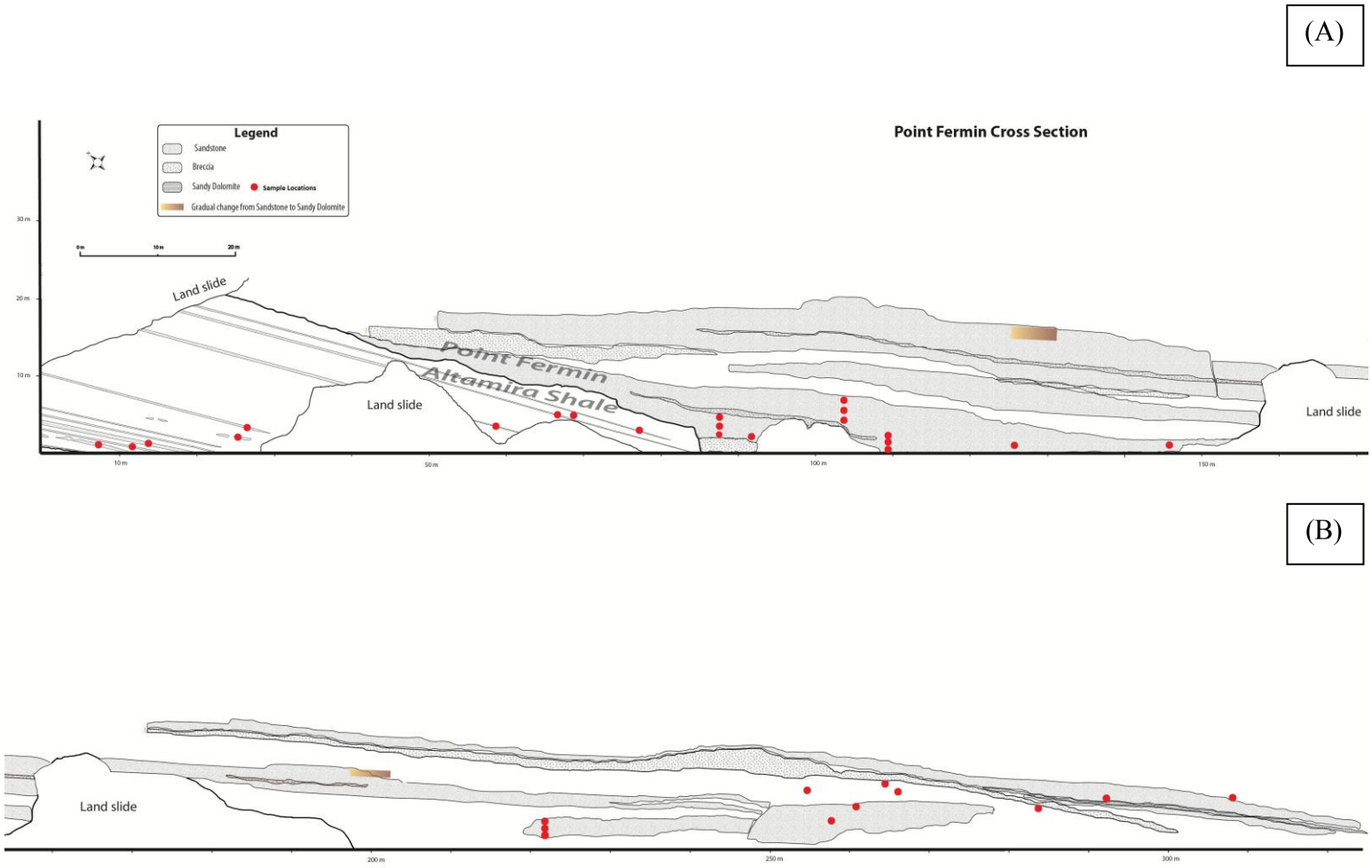
(A)
Point Fermin Cross Section
Legend
Sandstone
Breccia
Sandy Dolomite
Sample Locations
Gradual change from Sandstone to Sandy Dolomite
0m
10m
20m
30 m
20 m
10 m
Land slide
Point Fermin
Altamira Shale
Land slide
Land slide
10 m
50 m
100 m
150 m
(B)
Land slide
200 m
250 m
300 m

Stratigraphy

The apparent dip of the generally fine-grained Altamira Shale member is 17° to the south-southeast. In addition to the minor number of sandstones that are the focus of this study, other rocks in the Altamira Shale at this location include: sandy dolomite, siliceous shale, porcelanite and other minor rocks. In general, the grain size of the Altamira Shale units is very fine-fine and silty. Altamira Shale sandstone bodies are very thinly to medium-or rarely thick-bedded sandstones that are intercalated with other, finer-grained Altamira Shale lithologies. The Altamira Shale sandstones are generally grayish tan or light brown and only few sandstones beds contain coarse grains-most are poorly sorted with very fine grains. Eleven sandstone beds in the study area were identified based on the criteria that they had to be 10 cm thick or thicker. The thickness and lateral extent of the sandstone beds in the Altamira Shale are quite variable. Some beds are distinctly lenticular, up to 2 m wide and 20-50 cm thick. Some beds are fairly uniform in thickness and composition, while some grade to sandy dolomite both vertically and laterally. The approximate sandstone: shale or "sandy dolomite" ratio is 20%-30%.

Point Fermin sandstone is a thick to very thickly bedded coarse-grained unit that is in general has an overall lenticular shape that displays packages of thick, lenticular strata representing submarine channel deposits. Bedding has a general dip of around 15° to the south. The general color of Point Fermin sandstones is brown to dark brown and many beds have a strong petroliferous odor which prompted this research. The average thickness of the sandstone beds is ~ 2 m. The Point Fermin member is mostly sandstone with few breccia layers and some sandy dolomite layers. There is a large range in the sandstone grain size in the Point Fermin between and within graded beds; sediment

ranges from very fine to pebbly in size. Scour marks distinguish the bottom of the sandstone beds (FIGURE 5) and locally cut down several feet through several layers of underlying strata. Some sandstone beds gradually change to sandy dolomite laterally. Many of the sandstone beds thin or pinchout entirely on the south and north side while they are thicker in the center. The sandstone : shale or sandy dolomite ratio is 90%.

FIGURE 5. Scour marks in Point Fermin member.

Sample Locations

Nine samples were acquired from the eleven sandstone beds in the Altamira Shale that met the thickness criteria (thickness ≥10 cm). Some sandstone beds were so friable that a competent sample could not be acquired. One sample (AS-010) was obtained from a very dolomitic part of a sandstone bed to compare it with similar samples in Point

Fermin member (PF-150 and PF-151). FIGURE 6 shows three outcrop sample locations in the Altamira Shale member.

FIGURE 6. Outcrop photographs of three Altamira Shale sample locations.

Point Fermin samples were acquired to cover different parts of beds, both laterally and vertically, in submarine channel deposits. Samples were obtained close and far from the erosional contact with the Altamira Shale, in thickly bedded sandstone and in thinly bedded sandstone, as well as from the base and tops of thick graded beds. The difficulty in accessing the high, steep, vertical cliffs limited where samples in the Point Fermin could be acquired. FIGURE 7 displays the outcrops and stratigraphic character from which three samples from the Point Fermin member were taken.

Conventional Core Analysis

The conventional core analysis provided description of the samples, permeability, porosity, fluids saturation including oil, and grain density (TABLE 2). All but two of the Altamira Shale samples had 0% oil. Sample AS-01 had 5.7% oil, while AS-02 had 24.3% oil with respect to the pore volume, but with a porosity of only 4.6%. Because the percentage of oil can be misleading in high or low porosity rocks, a calculation of oil

volume/rock volume is useful. I calculated an oil percentage in rock volume based on the conventional core analysis data, as follows:

$$\frac{\text{Oil \%} * \text{Porosity \%}}{100}$$

The oil percentage of bulk rock volume for the Altamira Shale member sandstone samples is 0-1.12 %. This low range indicates that the Altamira Shale sandstones hold no to very little hydrocarbons.

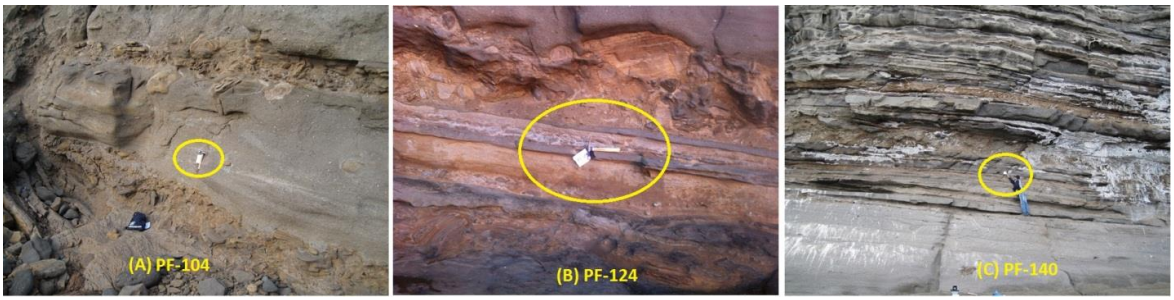

FIGURE 7. Outcrop photographs of three Point Fermin sample locations.

The permeability measurements must be reviewed with caution and are not indicative of pristine subsurface conditions because of fractures induced in collection and preparation of the samples or by surface weathering of the sandstone. One sample of the Altamira Shale (AS-010) is sandy dolomite, therefore cannot be compared to the other sandstone samples. Four of the eight Altamira Shale samples are fractured, in contrast to the Point Fermin samples which are mostly friable. As for the non-fractured samples in the Altamira Shale, the permeability ranges from 0.006 to 0.67 md (millidarcies). The porosity in the Altamira Shale ranges from 4.6-36.7 %. The average water saturation

percentage of the Altamira Shale samples is 36.3%. The average oil / water ratio is (0.07). The average grain density of the Altamira Shale samples is 2.68 g/cc.

In general, the Point Fermin member samples have good oil saturation. Twenty one samples were analyzed, two of which (PF-150 and PF-151) are sandy dolomite. The minimum oil percentage of the sandstone samples is 4.2%, the maximum is 56.3%, with an average oil saturation percentage for the Point Fermin member samples of 24.5%. The oil percentage in rock volume ranges from 1.05% to 21.92%, with an average of 7.74%.

The permeability measurements of the Point Fermin samples have the similar problems of outcrop fracturing. All the Point Fermin member sandstone samples are fractured except one sample PF-133. The porosity for the Point Fermin member sandstone samples have a minimum value of 11.6%, a maximum of 40.9%, and an average value of porosity of 30.1%. The average water saturation percentage in the Point Fermin samples is 15.8%. The average oil / water ratio is (2.0). The average grain density of the Point Fermin member samples is 2.82 g/cc. TABLE 2 shows the conventional core analysis data (take into account that AS-010, PF-150, and PF-151 are sandy dolomites). TABLE 3 shows the grain size range analysis for the thin sections.

Petrography

Thin sections were point counted by a modified Gazzi-Dickinson method to determine variation in provenance and to establish the types and degree of porosity and cementation. As described before, 32 samples were taken from the outcrops. Nine are from the Altamira Shale and 23 are from the Point Fermin unit. The 300 points were counted on all the samples except the sandy dolomite samples (AS-010, PF-150, and PF-151) because they are 95% dolomite and contain insufficient sand grains.

TABLE 2. Conventional Core Analysis, vf=very fine, f=fine, m=medium, c=coarse, vc=very coarse, gran=granule, pbly=pebbly, gr=grained, sst=sandstone, sltst, siltstone, lbrn=light brown, vslty=very silty, l=light, vis=visual, flor=florescence, gy= grey, dol=dolomitic, dgld=dull gold, blu=blue, sp=spotty, vdor=very dull odor, cly=clayey, vsdy=very sandy, scalc=slightly calcareous, calc=calcareous, tn=tan, stn= stain

Sample Number	Name	Perm. Kair md	Porosity %	Fluid Saturation				Grain Den g/cc	Mthd	Description
				Oil %	Water %	O/W Ratio	Total %			
1	AS-01	0.024	19.3	5.7	48.7	0.12	54.4	2.59	2	Sst lbrn vf-fgr vslty l stn no vis flor
2	AS-02	0.006	4.6	24.3	57.2	0.43	81.5	2.89	2	Sst gy vf-mgr vslty dol l stn dgld-blu flor
3	AS-07	F/ 238.0	31.7	0.0	27.5	0.00	27.5	2.55	2	Sst tn vfgr vslty no stn no flor
4	AS-008	F/ 234.5	36.7	0.0	32.3	0.00	32.3	2.58	2	Sst lbrn vf-gran vslty cly no stn no flor
5	AS-009	F/ 56.8	35.1	0.0	15.0	0.00	15.0	2.62	2	Sltst lbrn-tn vsdy cly scalc no stn no
6	AS-010	0.48	26.2	0.0	26.7	0.00	26.7	2.77	2	Sltst lbrn vsdy cly calc no stn no
7	AS-011	F/ 1967.1	34.5	0.0	28.6	0.00	28.6	2.76	2	Sst lbrn vf-f/vcgr vslty cly no stn no flor
8	AS-081	0.461	21.6	0.0	36.0	0.00	36.0	2.71	2	Sst gy-tn vf-fgr vslty no stn no flor
9	AS-033	0.67	24.2	0.0	45.0	0.00	45.0	2.76	2	Sst lbrn-tn vf-gran vslty scly no stn no flor
10	PF-104	F/ 67.6	25.3	4.2	39.7	0.10	43.9	2.83	2	Sst brn vf-pbly vslty m stn no vis flor
11	PF-105	F/ 202.2	40.9	20.3	14.8	1.37	35.1	2.80	2	Sst brn vf-vcgr vslty d stn no flor
12	PF-106	F/ 410.2	27.3	13.1	22.7	0.57	35.8	2.82	2	Sst brn vf-pbly vslty d stn vdgld flor
13	PF-116	F/ 2211.7	26.3	9.7	20.0	0.49	29.7	2.81	2	Sst lbrn-brn vf-pbly vslty scly lsp stn vdor-no vis flor
14	PF-117	F/ 927.7	34.6	14.2	15.1	0.94	29.3	2.80	2	Sst lbrn vf-pbly vslty scly m stn vdor-no vis flor
15	PF-118	F/ 225.0	32.2	14.5	18.2	0.80	32.7	2.79	2	Sst brn vf-pbly vslty scly m stn vdor flor
16	PF-119	F/ 381.8	26.9	10.3	18.2	0.56	28.5	2.79	2	Sst lbrn vf-pbly vslty lsp stn dgld flor
17	PF-120	F/ 1458.9	30.3	11.1	12.8	0.87	23.9	2.81	2	Sst lbrn vf-gran vslty m stn vdor-no vis flor
18	PF-121	F/ 1869.3	36.2	16.5	12.7	1.30	29.2	2.77	2	Sst dbrn-brn vf-vcgr vslty scly scalc d-m stn dgld

TABLE 2. Continued

Sample Number	Name	Perm. Kair md	Porosity %	Fluid Saturation Oil %	Water %	O/W Ratio	Total %	Grain Den g/cc	Mthd	Description
19	PF-123	F/ 560.9	34.1	43.7	9.8	4.48	53.5	2.78	2	Sst dbrn vf-vcgr slty d stn vdor flor
20	PF-124	F/ 1309.2	37.6	56.1	13.7	4.10	69.8	2.89	2	Sst dbrn vf-mgr vslty d stn vdor flor
21	PF-125	F/ 440.8	32.3	42.5	12.7	3.35	55.1	2.88	2	Sst dbrn vf-vcgr vslty d stn vdor flor
22	PF-126	F/ 549.3	27.7	16.3	20.4	0.80	36.7	2.80	2	Sst lbrn vf-pbly vslty scly m stn vdor-no vis flor
23	PF-127	F/ 453.3	30.2	20.0	15.8	1.27	35.7	2.79	2	Sst lbrn-dbrn vf-pbly vslty scly scalc m-d stn vdor
24	PF-128	F/ 434.8	36.2	19.1	12.1	1.57	31.2	2.78	2	Sst brn vf-gran vslty scly m-d stn vdor flor
25	PF-132	F/ 13.0	14.7	19.8	12.0	1.65	31.8	2.85	2	Sst lbrn vf-gran vslty scalc msp stn dgld flor
26	PF-133	2.6	11.6	23.9	19.4	1.23	43.3	2.85	2	Sst lbrn vf-gran vslty scly scalc msp stn dgld flor
27	PF-134	F/ 573.7	32.8	36.3	11.9	3.05	48.2	2.80	2	Sst dbrn vf-cgr vslty d stn vdor flor
28	PF-136	F/ 372.7	24.3	35.0	12.3	2.84	47.3	2.83	2	Sst dbrn vf-vcgr vslty d stn vdor flor
29	PF-140	F/ 254.8	31.7	32.1	10.4	3.08	42.5	2.90	2	Sst dbrn vf-gran vslty d stn vdor flor
30	PF-141	F/ 1771.0	39.0	56.3	7.5	7.50	63.8	2.88	2	Sst dbrn vf-mgr vslty d stn vdor-no vis flor
31	PF-150	6.3	25.9	4.3	21.5	0.20	25.8	2.72	2	Sltst brn svdy cly calc carb lsp stn no vis-vdor flor
32	PF-151	1.2	15.9	6.1	32.5	0.19	38.6	2.76	2	Sltst brn svdy cly calc carb lsp stn no vis-vdor flor

TABLE 3. Grain Size

	vf	f	m	c	vc	gran	peb
AS-001	■	■	■	■			
AS-002	■	■	■	■	■		
AS-003	■	■	■	■			
AS-008	■	■	■	■			
AS-009	■	■					
AS-011	■	■	■	■			
AS-081	■	■	■	■			
AS-033	■	■	■	■	■	■	
PF-104			■	■	■	■	■
PF-105	■	■	■	■	■		
PF-106	■	■	■	■	■	■	■
PF-116	■	■	■	■	■	■	■
PF-117	■	■	■	■	■	■	
PF-118	■	■	■	■	■	■	
PF-119		■	■	■	■	■	■
PF-120		■	■	■	■	■	
PF-121		■	■	■	■	■	
PF-123	■	■	■	■			
PF-124	■	■	■				
PF-125	■	■	■	■			
PF-126		■	■	■	■	■	■
PF-127		■	■	■	■	■	
PF-128	■	■	■	■	■	■	■
PF-132	■	■	■	■	■	■	■
PF-133	■	■	■	■	■	■	
PF-134	■	■	■	■	■		
PF-136	■	■	■	■	■		
PF-140	■	■	■	■	■	■	
PF-141	■	■	■				

The point count parameters and definitions are given in TABLE 4. The intragranular porosity (Pra) and oil (O) are extra counts that are not included in the 300 point counts needed for each sample. TABLE 5 and TABLE 6 show the point counting results of the Altamira Shale and Point Fermin samples, respectively.

Composition-Plots

The following parameters are used to create ternary plots for both the Altamira Shale member samples and the Point Fermin member samples. The following show the identification parameters that are based on the point counting in Table 5.

$Q = Qm + Qp$

$F = P + K$

$L = Ls + Lm + Lv$

$Lt = L + Qp$

The modified point counting parameters and the triangle diagrams are based on the works of Dickinson (1970), Graham et al. (1976), Ingersoll and Suczek (1979), Ingersoll et al. (1984), Graham and Midgley (2000), Tucker (2001), and Garzanti and Vezzoli (2003).

IGV

Intergranular volume (IGV) is a measurement of the degree of compaction. It measures the space between the grains (Paxton et al, 2002). The IGV formula is

$$\text{IGV (Volume \%)} = \text{V intergranular porosity} + \text{V intergranular cement} + (\text{V detrital matrix})$$

(Milliken et al., 2007)

Where (V) means volume

TABLE 4. Definitions of Point Count Parameters

Point count symbol	Definition
Qp	Polycrystalline Quartz
Qm	Monocrystalline Quartz
P	Plagioclase
K	Potassium Feldspar
Ls	Sedimentary Lithic
Lm	Metamorphic Lithic
Lv	Volcanic Lithic
Cc	Carbonate Cement
Cl	Clay Cement
Cs	Secondary Cement
Pi	Intergranular Porosity
Pf	Fracture Porosity
F	Fossil
Misc	Miscellaneous
Pra	Intragranular Porosity
O	Oil

TABLE 5. Altamira Shale Point Counting

Sample	AS-001	AS-002	AS-003	AS-033	AS-008	AS-009	AS-010	AS-011	AS-081
Point Counting									
Remarks							95% Cc		
Qp	19	25	43	31	43	23	0	15	18
Qm	12	9	15	3	17	26	0	15	22
P	2	0	0	2	2	0	0	1	3
K	3	2	4	0	1	3	0	2	4
Ls	13	45	15	25	9	2	0	17	22
Lm	75	60	42	96	60	8	0	56	76
Lv	4	6	0	13	0	3	0	1	13
Cc	52	131	2	0	0	213	0	113	0
Cl	0	0	118	11	100	0	0	52	0
Cz	0	0	18	49	3	0	0	10	57
Pi	0	1	3	0	6	13	0	2	6
Pf	0	0	0	0	0	0	0		0
Fs	2	0	0	0	0	0	0	0	0
Misc	118	16	43	27	55	7	0	11	31
Pra	8	3	18	13	33	2	0	0	54
O	6	4	1	6	68	0	0	62	5

TABLE 6. Point Fermin Point Counting

Sample	PF-104	PF-105	PF-106	PF-116	PF-117	PF-118	PF-119	PF-120	PF-121	PF-123	PF-124	PF-125	PF-126	PF-127	PF-128	PF-132	PF-133	PF-134	PF-136	PF-140	PF-141	PF-150	PF-151
Point Counting																						Cc 95%	Cc 95%
Remarks																							
Qp	56	42	70	45	58	61	67	67	56	65	27	51	126	58	63	42	57	60	62	25	21	0	0
Qm	7	6	5	2	8	13	2	6	12	6	7	10	6	4	5	1	3	5	2	4	13	0	0
P	2	2	1	3	0	0	0	2	2	2	4	2	0	4	1	0	4	3	2	1	2	0	0
K	2	1	0	1	1	4	0	2	0	0	0	0	2	5	6	2	4	0	2	1	4	0	0
Ls	66	22	27	41	68	63	87	50	34	35	16	32	54	16	7	27	8	6	12	14	15	0	0
Lm	55	75	54	93	27	48	37	57	45	78	94	65	13	78	119	113	106	77	93	144	115	0	0
Lv	1	2	4	5	5	6	8	19	11	12	22	16	2	12	4	5	9	9	16	16	14	0	0
Cc	98	55	50	74	67	64	82	81	61	0	0	59	82	65	0	93	87	45	60	19	3	0	0
Cl	2	3	30	2	0	0	4	0	0	1	6	1	0	3	17	0	3	3	2	2	2	0	0
Cz	6	0	9	9	10	7	4	8	5	10	6	7	0	14	25	8	1	13	0	10	9	0	0
Pi	20	44	35	28	33	16	4	8	20	86	68	50	13	22	20	5	6	28	42	52	87	0	0
Pf	0	0	0	0	0	0	0	0	0	0	0	0	0	0	0	0	0	0	0	0	0	0	0
Fs	0	0	0	0	0	0	0	0	1	0	0	0	0	0	0	0	0	0	0	0	0	0	0
Misc	10	48	15	11	4	1	6	7	8	7	6	7	2	21	28	4	10	50	8	12	15	0	0
Pra	8	4	3	6	4	0	14	6	6	0	0	0	2	4	0	1	1	1	6	2	1	0	0
O	42	59	49	47	15	16	20	18	28	52	44	49	10	17	20	0	4	57	43	44	67	0	0

In my research, intergranular porosity (Pin) is equal to intergranular porosity + fracture porosity

$$\mathrm{Pin} = \mathrm{Pi} + \mathrm{Pf}$$

The intragranular porosity (Pra) is not included because it is part of the grains. The sum of (Pi) and (Pf) which is (Pin) is divided on the total count. The total point count that any measurement is normalized to the sum all point counts (300). On the other hand, total cement (C) is the sum of carbonate cement (Cc), clay cement (Cl), and secondary cement (Cs) that includes both zeolite cement and gypsum cement.

$$\mathrm{C} = \mathrm{Cc} + \mathrm{Cl} + \mathrm{Cs}$$

The sum is normalized to 100 by the same method mentioned before. The IGV values are given in TABLE 7. IGV was calculated using the intergranular porosity (Pin) volume and total cement (C) volume. The percentage of Pin and C of all the samples is given in TABLE 7 too.

TABLE 7. IGV Values and Intragranular Porosity (Pin) Percentage and Total Cement (C) Percentage

Sample	IGV	Pin %	C %
AS-001	17	0	17
AS-002	45	0	44
AS-003	47	1	46
AS-033	23	0	23
AS-008	37	2	35
AS-009	76	4	71
AS-011	60	1	59
AS-081	25	2	23
PF-104	39	6	33
PF-105	34	15	19
PF-106	41	12	30
PF-116	36	9	27
PF-117	39	12	27
PF-118	31	6	25
PF-119	31	1	30
PF-120	32	3	29
PF-121	34	8	26
PF-123	32	28	4
PF-124	31	27	5
PF-125	39	17	22
PF-126	32	4	27
PF-127	34	7	27
PF-128	21	7	14
PF-132	35	2	34
PF-133	33	2	31
PF-134	30	9	20
PF-136	35	14	21
PF-140	28	17	10
PF-141	34	29	5

CHAPTER 5

DISCUSSION

Sandstone Beds Interpretation

The Altamira Shale member is predominantly thin-bedded. Most of the sandstone beds are also and laterally continuous, although some grade to more dolomitic lithologies (FIGURE 8-A). Sharp tops and bases, some textural grading and intercalation with fine-grained lithologies suggest that the sandstones are mostly turbidites deposited in a deep, hemi-pelagic setting. In contrast, the Point Fermin member sandstones and breccias are thickly bedded, coarser grained and clearly graded, many with scoured, irregular bases (FIGURE 8-B). Their overall lenticular geometry and sharp termination against the eroded contact with the underlying Altamira Shale indicate that the Point Fermin sandstone is submarine channel deposit. The overall level of depositional energy was high in the Point Fermin channel and low during deposition of the Altamira Shale member. This is shown by the difference in grain size between the two and the abundance of erosional features.

Depositional Relationships

There is a subtle difference in apparent dip between the Altamira Shale and Point Fermin members, with the Altamira Shale strata at ~17° and the Point Fermin beds at ~15°. This difference likely reflects the difference in plunge between the downcutting channel and the pre-existing slope.

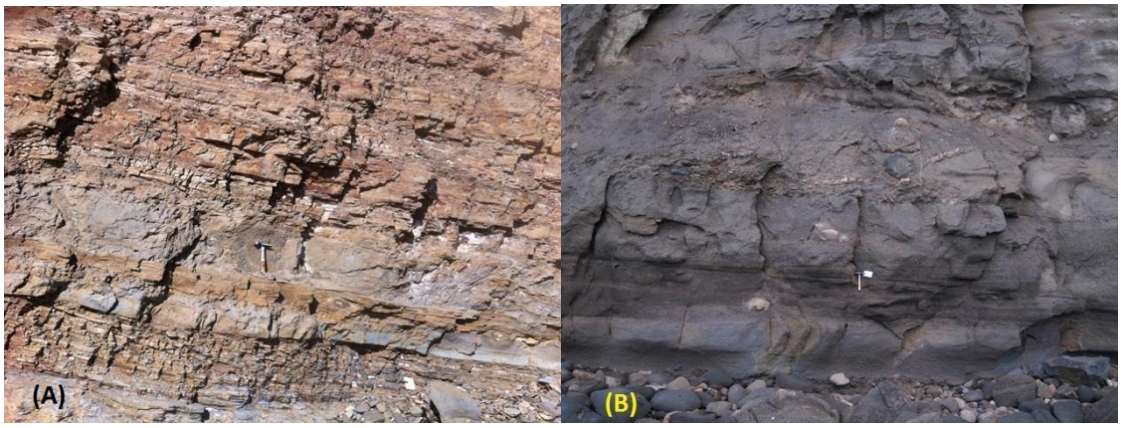

FIGURE 8. (A) Altamira Shale thin beds (B) Point Fermin thick beds.

There are numerous breccia beds in the Point Fermin member. They are generally lenticular and thin to the northern and southern direction. The breccia clasts are mainly sedimentary or metamorphic rocks (shale, dolostone, phosphate, schist and bone fragments). FIGURE 9 show coarse-grained high energy deposits that are normally graded.

In outcrop, large pebble to boulder size sedimentary clasts, principally with distinct Monterey type lithologies are more abundant nearer the base and eroded bank of the channel, and the relative abundance of metamorphic clasts increases with distance from the contact. This relationship likely reflects erosion and entrainment of Altamira Shale material quite proximal to the depositional site, whereas erosion and entrainment of the metamorphic clasts from exposures of the Catalina Schist occurred farther away. A similar relationship is shown in the sand-size fraction in thin section. FIGURE 10 displays a plot for close-to-contact Point Fermin samples (PF-116, PF-117, and PF-118) that are 10-20 meters from contact, versus far-from-contact samples (PF-136, PF-140,

and PF-141) that are 160-220 meters from contact. The percentage of Ls and Lm are based on the total lithic grains in each sample (L).

FIGURE 9. Coarse-grained, high-energy submarine channel deposits.

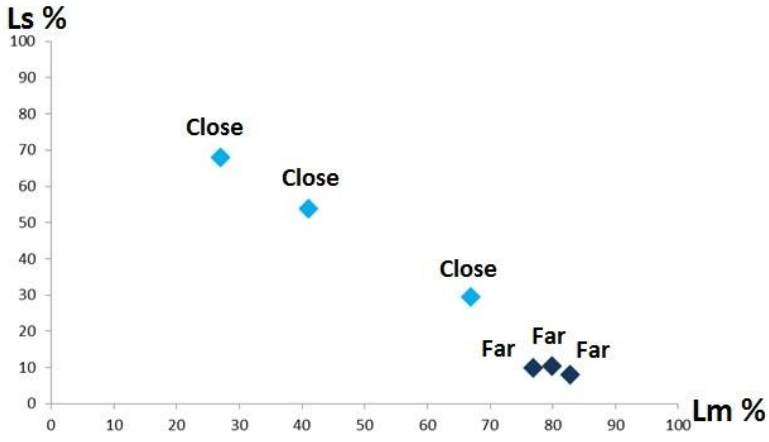

FIGURE 10. Distribution of sedimentary vs. metamorphic lithic grains with respect to position.

Provenance

The point counting yielded important information about the provenance of the Altamira Shale member and the Point Fermin member. Petrographic analysis of thin

section of sandstones from the two members suggest that they have similar compositions. They are both litharenites. The Q-F-L ternary diagram shows that both the Altamira Shale and Point Fermin members have the same provenance (FIGURE 11). The plot intensity for the Point Fermin is greater in that it includes are 21 samples, while the Altamira Shale has only 8.

Based on Dickinson and Suczek (1979) and Suttner and Dutta (1986), the plotting in this compositional field on the ternary diagram indicates that the source was metamorphic and that deposition may have occurred in an arid climate. High relief probably contributed to a short transport distance where any weathering would likely have been more mechanical than chemical for these grains.

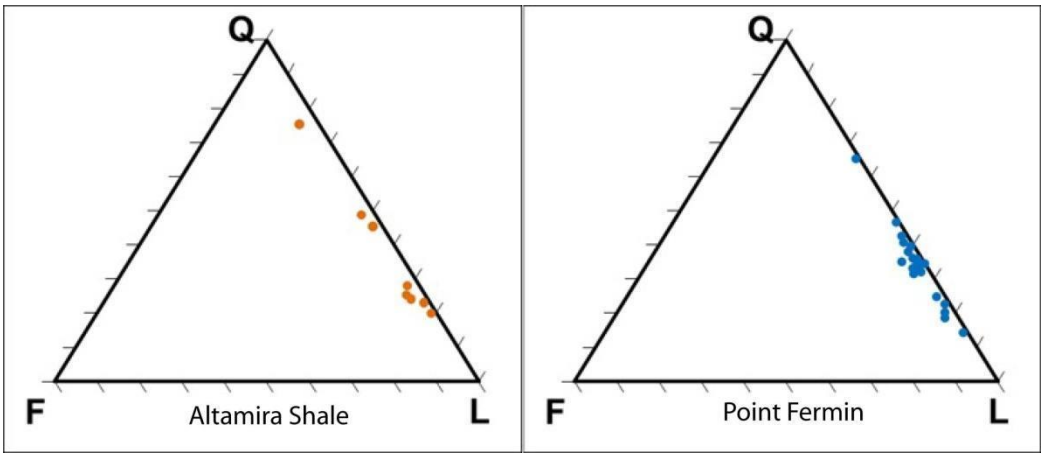

FIGURE 11. Q-F-L ternary diagram.

The Qm-F-Lt triangular diagram is used to differentiate the provenance terranes (FIGURE 12) and indicates both members are from recycled orogeny provenance (Dickinson and Suczek, 1979). Such provenances are either from continent to continent

collision or ocean to continent collisions (Dickinson and Suczek, 1979). The latter is the case for coastal California. Some Qm grains actually are pieces of Qp grains that were fragmented, as I have noticed in some thin sections, and which is addressed elsewhere in this paper.

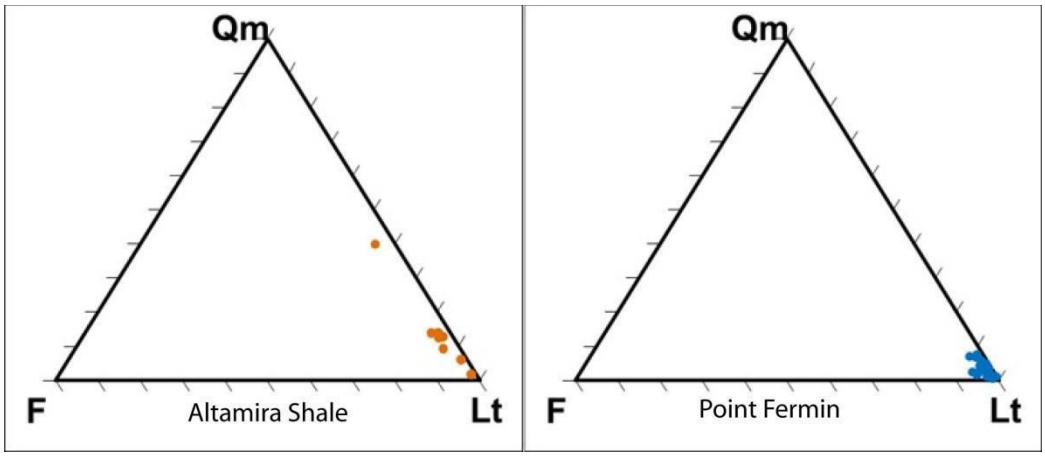

FIGURE 12. Qm-F-Lt ternary diagram.

The Lm-Lv-Ls diagram indicates similarities and small differences between the members (FIGURE 13). Most samples have higher percentage of Lm grains because of the "Catalina Schist" source. Some samples in the Point Fermin unit have higher Ls grains because they are closer to the contact between the two members (compare with Figure 10). These early or lower deposits of the submarine channel cut through and incorporated underlying Monterey deposits, explaining the higher percentage of Ls in these Point Fermin samples.

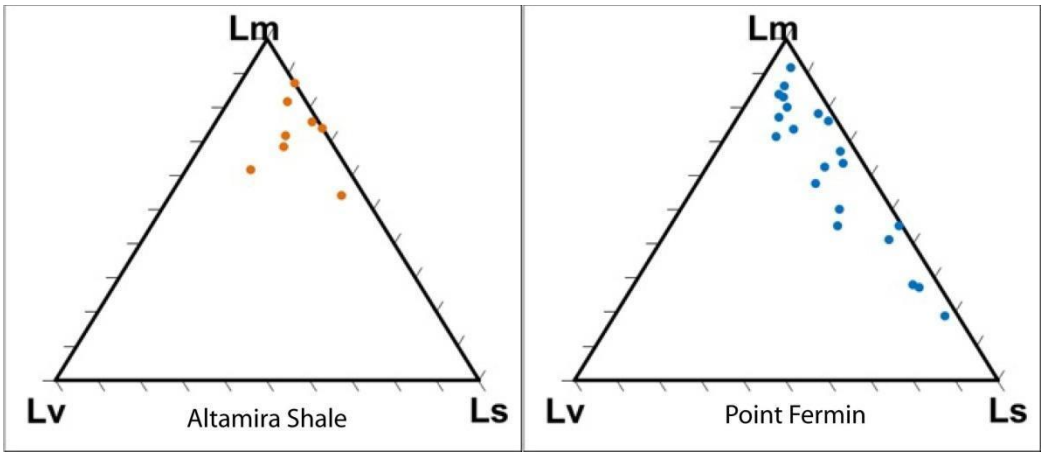

FIGURE 13. Lm-Lv-Ls ternary diagram.

All the Q-F-L, Qm-F-Lt, and Lm-Lv-Ls diagrams confirm that the Altamira Shale and Point Fermin members have the same provenance-the Catalina Schist. The Catalina Schist is exposed not far away from the Point Fermin locality at the Catalina Islands and at a small area north of Point Fermin in the Palos Verdes Hills.

Relation between Qm and Qp

Most of the quartz that is present in the thin sections of both the Altamira Shale and Point Fermin is polycrystalline quartz (FIGURE 14). This is typical of metamorphic rock, which in the study area is the Catalina Schist-provenance for both members. There are few monocrystalline quartz grains

FIGURE 15).

Many of these monocrystalline quartz were not deposited that way, but are a result of disintegration of polycrystalline quartz grains. This disintegration is evident in some thin sections (FIGURE 16). Another confirmation is that polycrystalline grains are coarser than the monocrystalline grains and that monocrystalline quartz grains are present mostly in very fine sediment samples. If the monocrystalline quartz is original, we would

assume that the particles will be of the same size or larger than the polycrystalline quartz because of their greater mechanical stability.

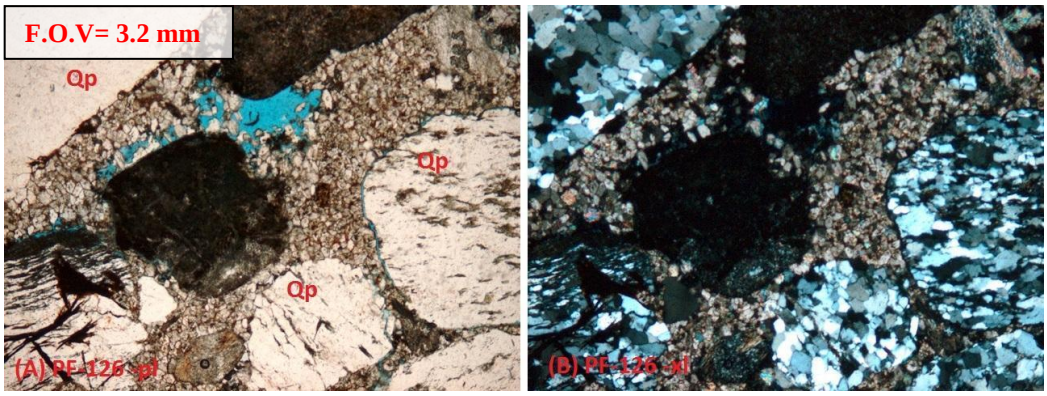

FIGURE 14. Polycrystalline quartz grains (F.O.V = field of view, pl = plain light, xl = cross polarized light).

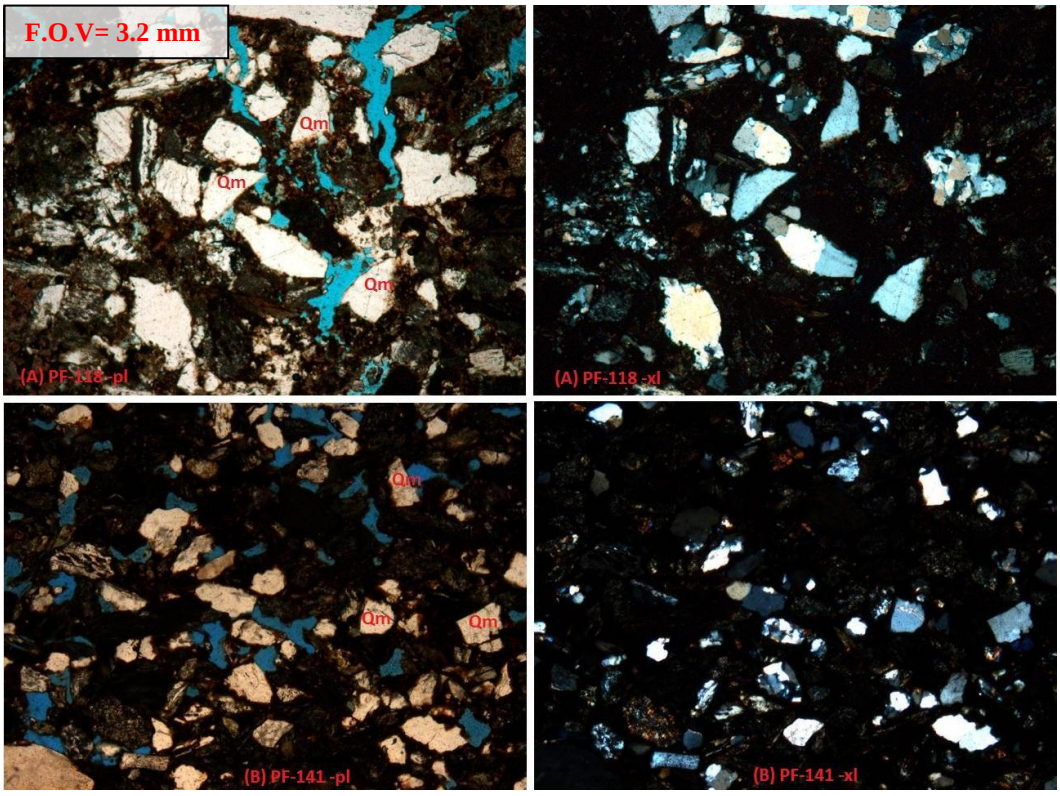

FIGURE 15. Monocrystalline quartz grains.

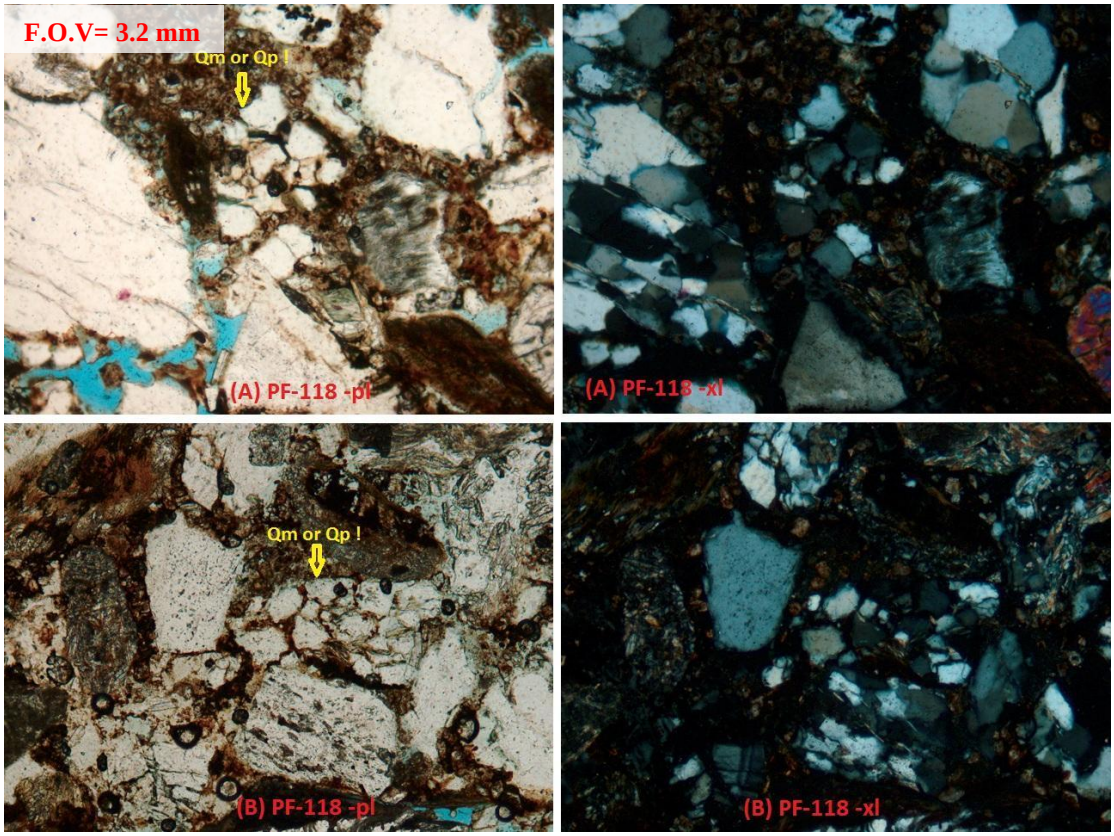

FIGURE 16. Disintegration of polycrystalline to fragments of monocrystalline quartz.

Sandstone to Dolomite Ratio

To describe trends in most clastic systems, geologists use the sandstone to shale ratio, but in the special case at Point Fermin sandstone, the sandstone also changes laterally to dolomite or is interbedded with sandy dolomite, in addition to clastic shale. The sandstone: shale/sandy dolomite ratio in Altamira Shale is around 20%-30%, while in the Point Fermin it is around 90%. The ratio reflects a marked difference in sedimentary and geochemical environment that might have affected sandstone cementation and diagenesis. Beds overlying and underlying each sandstone may would have influenced the geochemistry of pore fluids in the sandstone, especially when they are volumetrically much larger. Localized differences in sediment ratios may help

explain variation in sandstone cement, both within and between each member. Secondary zeolitic cement and less carbonate occurs in some of Altamira Shale samples (AS-081, AS-033, and AS-03). While Point Fermin sandstones contain mostly dolomite cement, some samples are uncemented, for example (PF-123, PF-124, and PF-140).

Sandy Dolomite Samples and Depositional Mechanisms of Dolomite Matrix/Cement

Three sandy dolomite samples were analyzed, one taken from Altamira Shale member (AS-010) (FIGURE 17-A) and two from Point Fermin member (PF-150 and PF-151) (FIGURE 17-B and C). The sandstone grades both vertically and laterally to dolomite in some beds. FIGURE 18 is a thin section for the samples AS-010, PF-150, and PF-151. The sandy dolomites contain up to 95% dolomite. The dolomite carbonate cement in the sandstone samples (FIGURE 19) is identical to that in the sandy dolomite. The dolomite has angular, subhedral rhombohedral crystals. The dolomite crystals could not have been transported, otherwise the sharp angular edges of the crystals would have been rounded or broken. The best explanation is that this matrix was composed of very fine chemically unstable components, like diatoms and sponge spicules, which have an extremely high porosity of approximately 70-80%, and that they were dolomitized by magnesium-rich, sulfate-poor water. This must have happened near the sediment - water interface because the grains are not compacted.

Origin of Dolomite

Spotts and Silverman (1966) concluded that the dolomite has an organic origin in Point Fermin based on the fact that most of the dolomite crystals had hydrocarbon nuclei. I also observed many dolomite crystals with hydrocarbon nuclei (FIGURE 20).

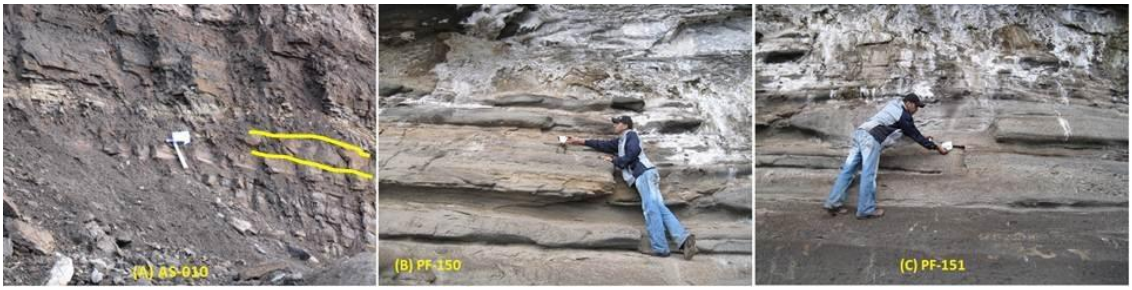

FIGURE 17. Sandy dolomite beds (A) AS-010, (B) PF-150, (C) PF-151.

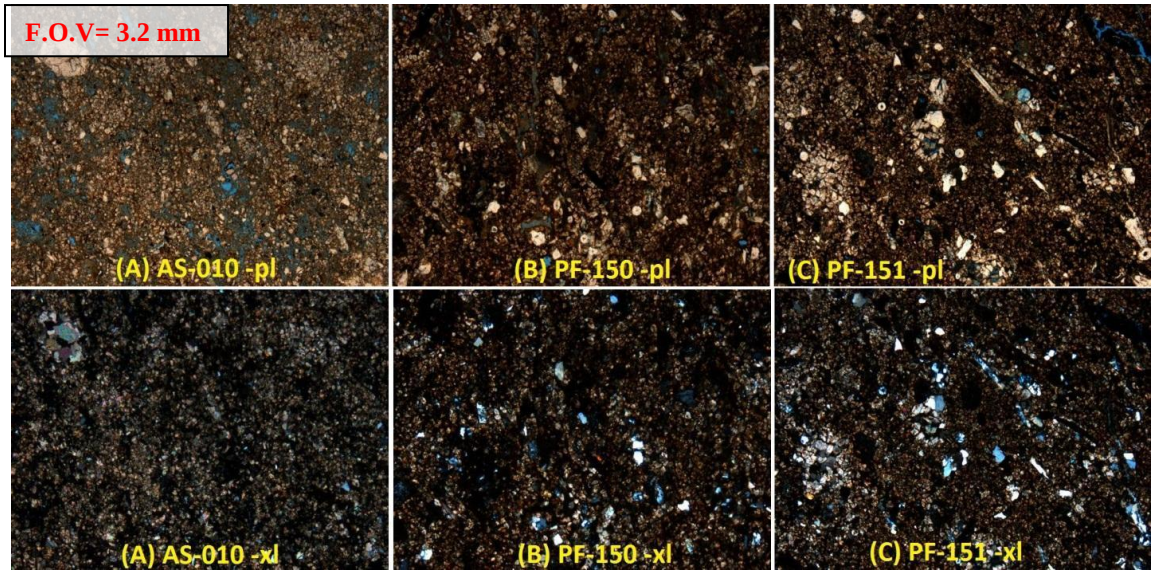

FIGURE 18. Sandy dolomite photomicrographs (A) AS-010 (B) PF-150 (C) PF-151.

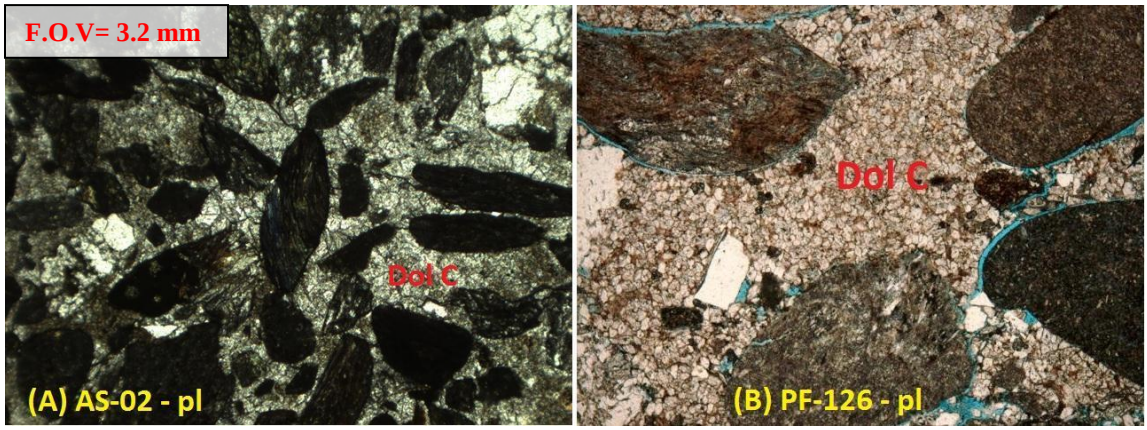

FIGURE 19. Floating grains in dolomite cement (pl = plain light).

It is observed that the sandy dolomite samples (AS-010, PF-150, and PF-151) have abundant sponge spicules (FIGURE 21). They must have deposited during an interval of prolific growth of sponges in the local benthic environment, or they were transported from their original environment of growth to the Point Fermin submarine channel, as their ultimate depositional environment. A highly biosiliceous, sandy deposit such as a spiculite would provide enormous initial porosity that was ultimately filled by authigenic dolomite cement. In just a porous microenvironment, dolomite crystals would be free to grow into whatever habit is mandated by the pore water chemistry without substantial early interference by crowding by other grains. In Point Fermin, all of the dolomite crystals are rhombohedral to anhedral in shape (FIGURE 22).

Based on studies of other locations (Spotts and Silverman, 1966; Nielson et al., 1997; Cavagna et al., 1999; Gunatilaka, 1989), dolomite that is associated with hydrocarbon nuclei can be subdivided to two types: rhombohedral and spherical. There is no clear explanation why dolomite with hydrocarbon nuclei would have one or either of these two habits - rhombohedral or spherical - but their formation is thought to be associated with methanogenesis and sulfate reduction at shallow burial depths (Shimmield and Price, 1984; Suess, et al., 1988; Wafer et al., 1998; Fayek et al., 2001). Bacteria almost certainly play an important role in the formation of dolomite and the presence of hydrocarbon micro droplets would provide and important source of energy for their metabolism , with the byproduct of creating the optimal environment for dolomitization (Roehl, 1981; Wright and Wacey, 2005). Consequently, the occurrence of dolomite with hydrocarbon nuclei can be a good indicator of an active petroleum system during their diagenesis and an indicator of the possibility of other hydrocarbon traps

because the oil or gas present as nuclei must have been seeps from deeper sources and potential reservoirs (Gunatilaka, 1989).

First Phase and Second Phase Dolomite Diagenesis

Uncemented sandstone is an ideal hydrocarbon reservoir, but this is rarely the case for rocks millions of years old. In an era in which unconventional reservoirs are gaining importance, understanding less ideal reservoirs is increasingly important.

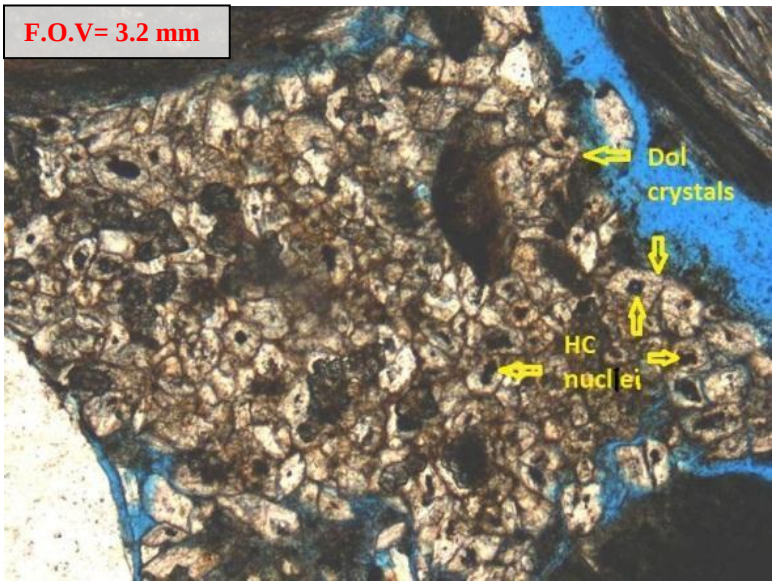

FIGURE 20. Dolomite crystals with hydrocarbon nuclei.

Samples from the Point Fermin study are that are mostly dolomite cemented still have good oil saturations. The subhedral to rhombohedral dolomite cement crystals generally preserve some porosity and permeability. However, some of the samples (or parts of them) went through a second phase of diagenesis, in which the space between the dolomite crystals decrease with the coalescence of growing crystals, giving them an irregular and anhedral form. The porosity and permeability decreases as a result.

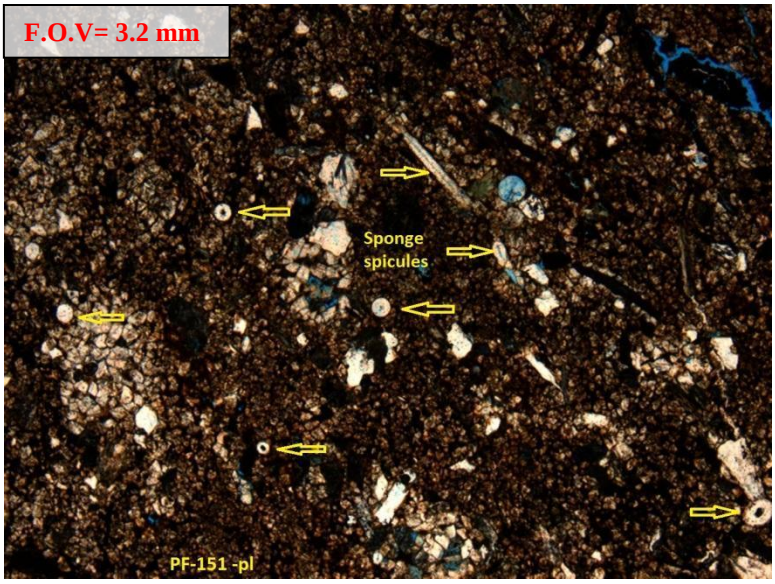

FIGURE 21. Sponge spicules in sandy dolomite.

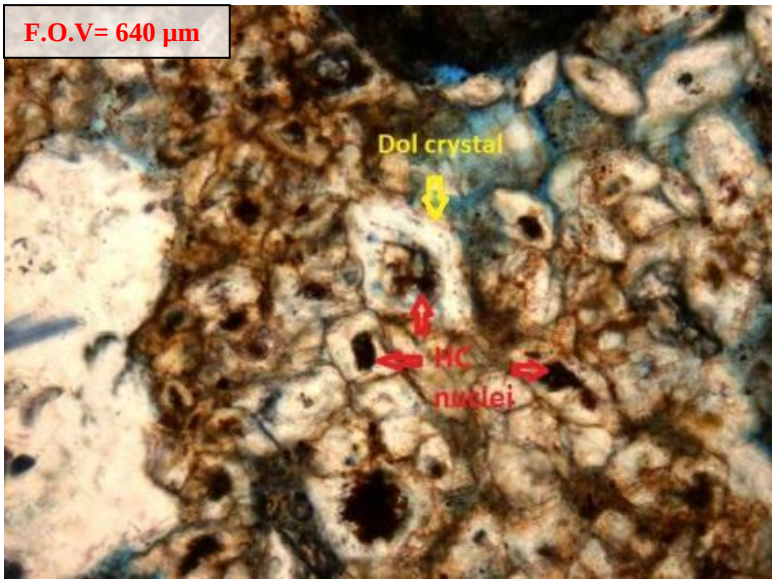

FIGURE 22. Dolomite crystals with hydrocarbon nuclei and incorporating hydrocarbons in some successive crystal growth layers.

The Altamira Shale samples show some degree of this second phase diagenesis while Point Fermin samples are more rhombohedral (FIGURE 23), and this assists in explaining the difference in oil saturation between the two members. FIGURE 24 is an example of the dolomite cement crystals with second phase diagenesis. Two features

characterize the second phase of diagenesis: first, an absence of hydrocarbons in this phase of the crystals; and second, the loss of the rhombohedral crystal shape of the dolomite crystal. FIGURE 25 is a sketch of how the dolomite crystal goes through a second phase of growth.

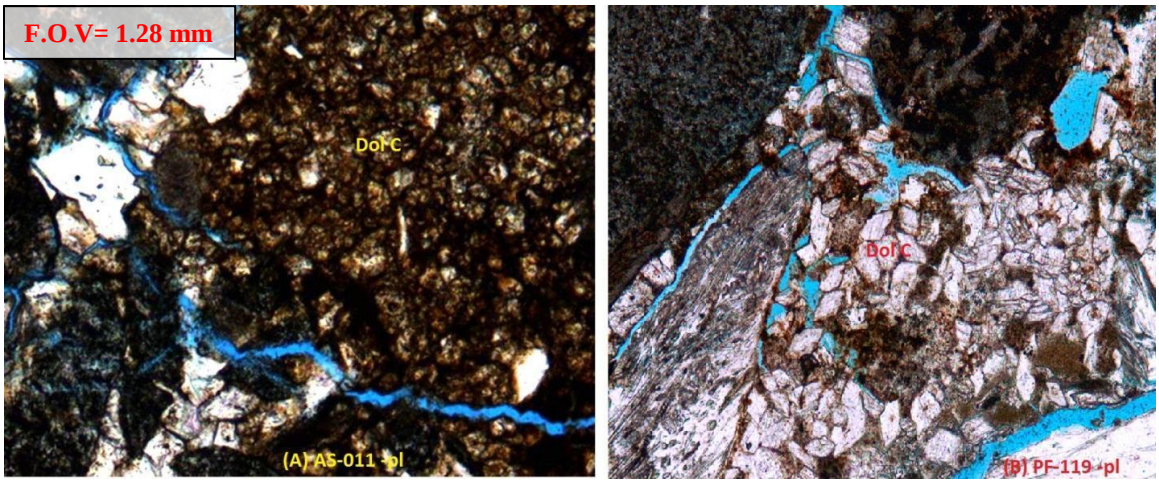

FIGURE 23. Point Fermin has more rhombohedral crystals shape than the Altamira Shale.

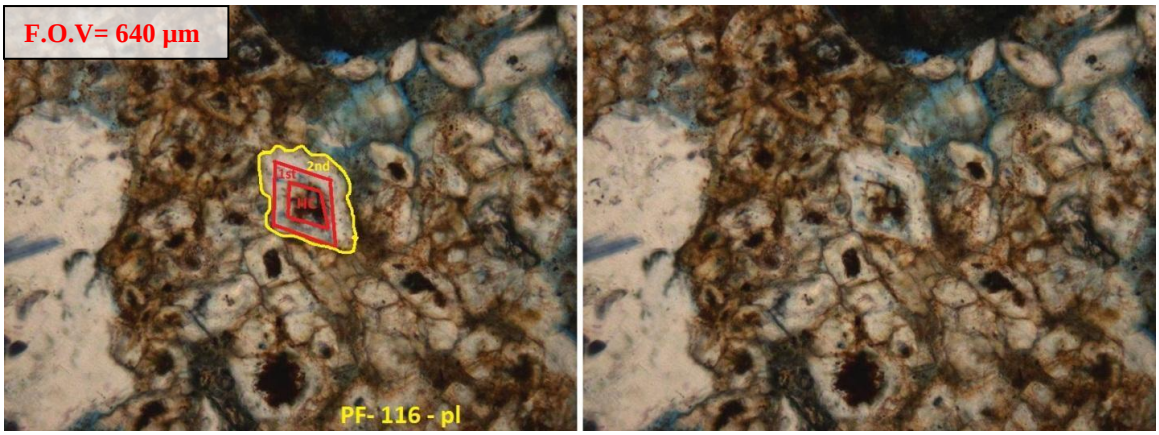

FIGURE 24. Second phase of dolomite crystal growth without hydrocarbon inclusions in outer, anhedral rims.

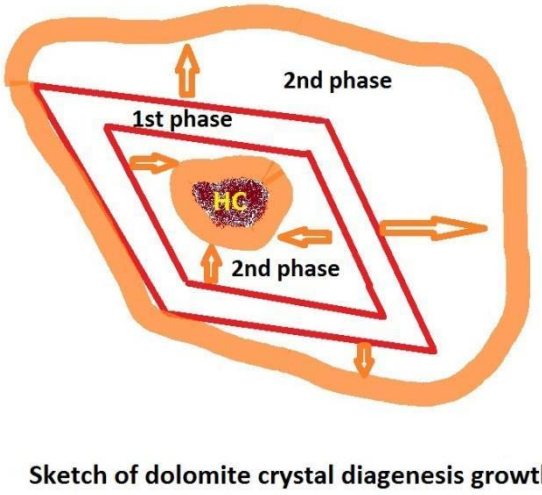

FIGURE 25. Sketch of dolomite crystal diagenesis growth.

Dolomite and Calcite Cement

Interstitial cement is mostly carbonate and primarily dolomite. In some samples, coarsely crystalline calcite cement is surrounded by much finer dolomite cement, the calcite apparently filling later stage voids (FIGURE 26).

The thin section of one sample (AS-011) shows very thin, sub-millimeter-scale, laminations with alternating dolomite cement and calcite cement (FIGURE 27). Distinct diagenesis on this small spatial scale suggests that primary, short-term variations in sediment composition or texture can differently influence pathways of post-depositional alteration, resulting in a complex rock or reservoir. The calcite cement seems to be associated with the most sandy layers and the dolomite with the layers with little or no sand. This suggests that the calcite was associated with lamination with greater permeability that may have been less susceptible to maintenance of a reduced, sulfate-poor microenvironment. These mineralogic variations can be evidence of how important

the geochemistry of the matrix may be in controlling the pore water composition for dolomite precipitation.

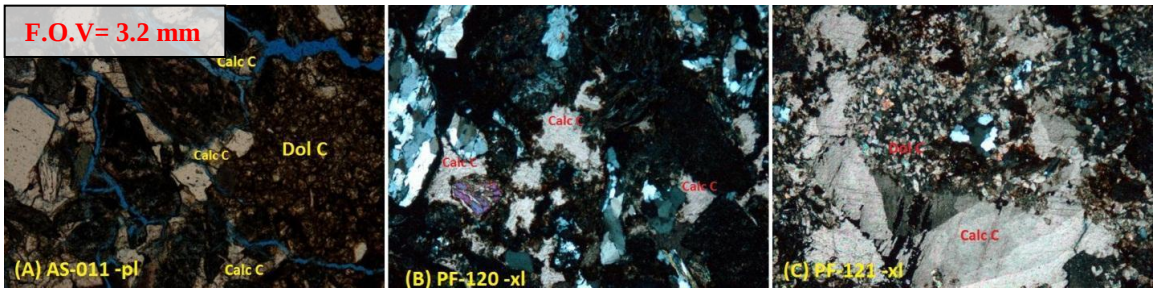

FIGURE 26. Dolomite cement and calcite cement.

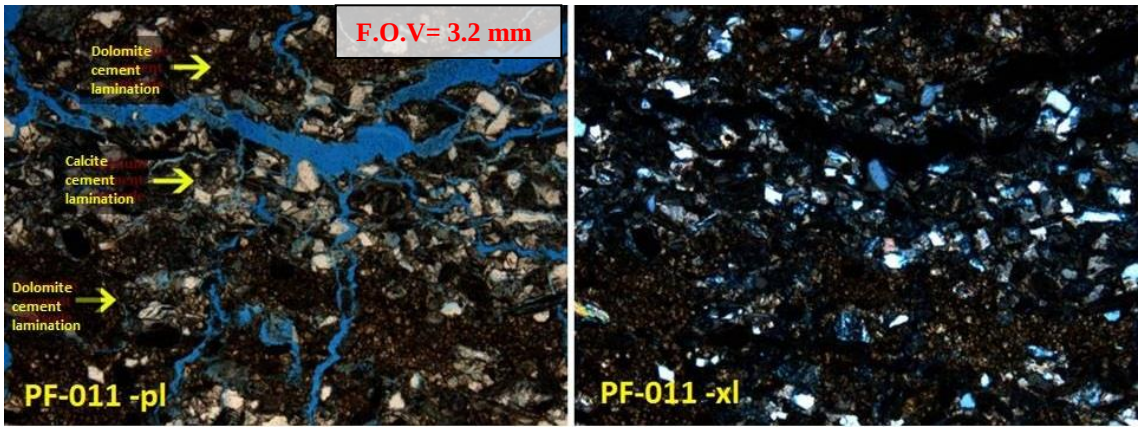

FIGURE 27. Dolomite and calcite cement laminations.

Zeolite and Gypsum Cements

Later stage cementing minerals - zeolite and gypsum - fill fractures in the sandstones. Zeolite is formed mainly by the alteration of volcanic material (Deffeyes, 1959). There was intermittent volcanic activity during the middle to late Miocene in this vicinity that ceased around 12-14 Ma (Schwartz and Colburn, 1987) and, as previously discussed, the thickest of the subdivisions of the Altamira Shale is the tuffaceous

lithofacies of Conrad and Ehlig (1983). This lithofacies was primarily deposited prior to the Point Fermin Sandstone and would have provided some of the sedimentary material eroded by turbidity currents in the downcutting channel. Some tuff beds are present even in overlying facies (e.g., Valmonte Diatomite) that are younger than the Point Fermin Sandstone. Volcanic rock fragments make up 0-13% of the sandstone framework grains (Figure 13). Zeolite diagenesis in sedimentary successions generally occurs with deeper burial depths and requires higher temperature (~90°C) (Noh and Boles, 1993). The zeolite cement is most common (though never abundant) in the Altamira Shale samples and reflects diagenesis at greater burial than the carbonate cements (FIGURE 28) (Deffeyes, 1959; Noh and Boles, 1993). In Point Fermin member, the zeolite cement is rare, whereas gypsum is found in similar locations surrounding grains at their boundaries (FIGURE 29). In some cases, the gypsum cement extends and fills in more extensive pores or cross-cutting fractures (FIGURE 30). Both mineral cements are late diagenetic features, but cross-cutting relationships indicate that the zeolite preceded the gypsum, with the latter almost certainly being a surficial weathering precipitate, common in sulfur-rich rocks containing organic matter or hydrocarbons. These late-stage cements only partly fill remaining voids, and porosity remains good in the Point Fermin member, allowing the sandstone to be charged with oil.

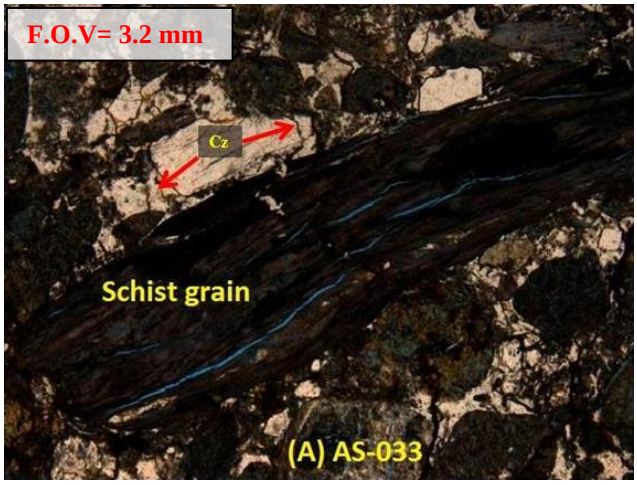

FIGURE 28. Zeolite cement in Altamira Shale, Cz: zeolite cement

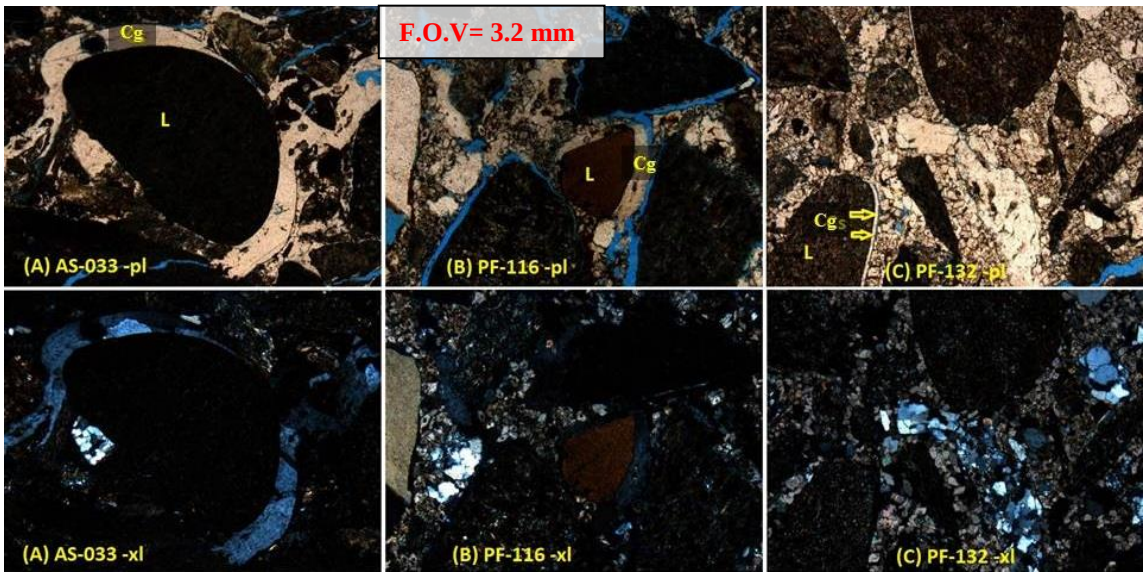

FIGURE 29. Gypsum cement around lithic grains (A) AS-033, (B) PF-116, (C) PF-132. L= lithic grain, Cg = gypsum cement.

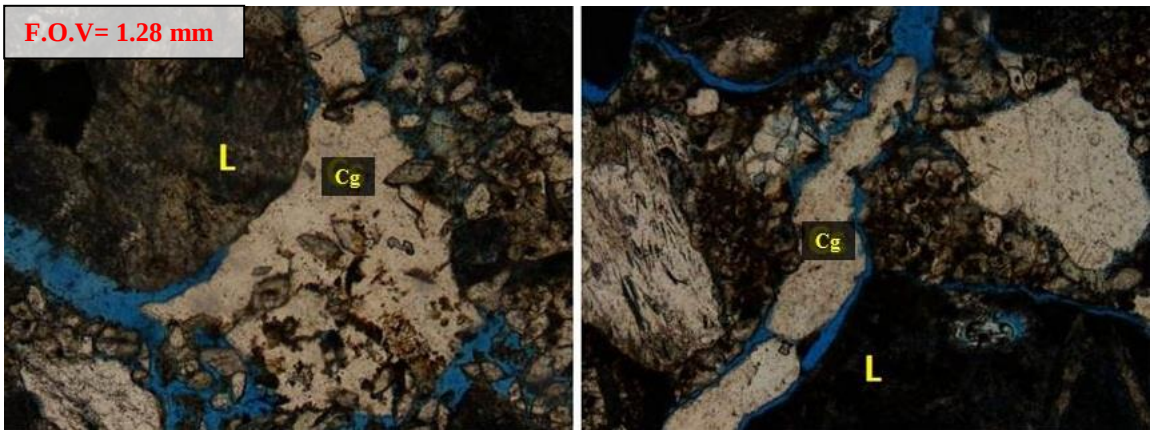

FIGURE 30. Gypsum cement filling fractures, L= lithic grain, Cg = gypsum cement.

Timing of Zeolite and Gypsum Cements

The coexistence of rhombohedral dolomite, anhedral dolomite, calcite, carbonate cement , zeolites, and gypsum (FIGURE 31) in many samples assists determination of the relative sequence of cement precipitation. Based on the relation we see in more than one sample, the carbonate cements (subhedral rhombohedral dolomite, anhedral dolomite, and calcite) are older than the zeolite and gypsum cements. FIGURE 31 shows the relation between the zeolite cement and the carbonate cement in which some dolomite crystals are of a rhombohedral shape, and were surrounded by late cement precipitation. Zeolite and/or gypsum cement also fills fractures that cut pre-existing dolomite cement (FIGURE 32), showing their relative age. All these indicators confirm that the dolomite and calcite cements precipitated earlier than the secondary cement of zeolite, then gypsum.

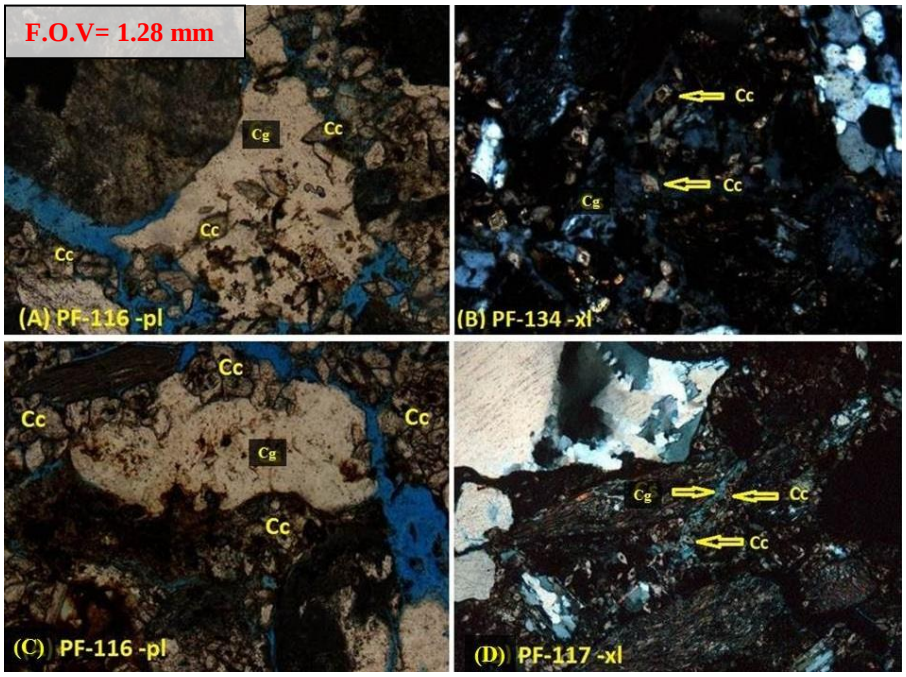

FIGURE 31. Relation between rhombohedral dolomite cement and gypsum cement, Cc = dolomite cement, Cg = gypsum cement.

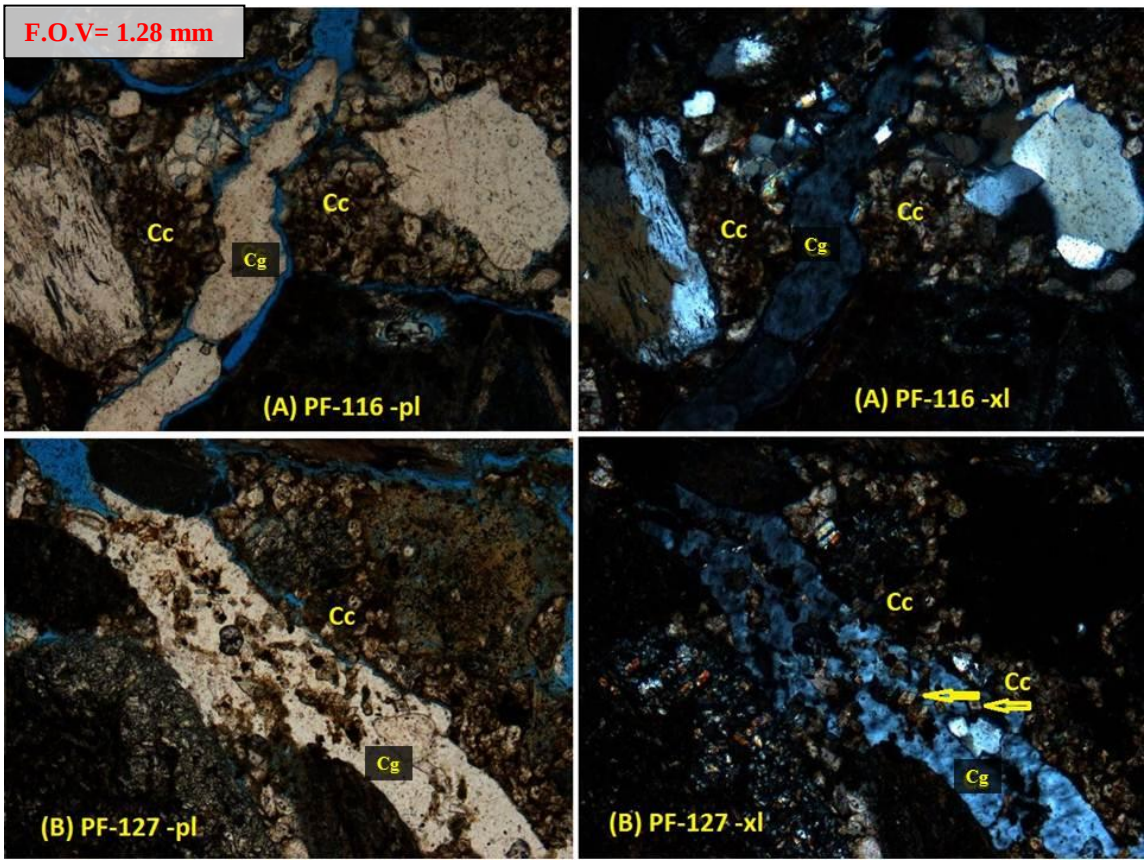

FIGURE 32. Gypsum cement cuts dolomite cement.

Cementation, Porosity, and Oil Saturation

The 32 sandstone samples from the Altamira Shale and Point Fermin members present an opportunity to study the different kinds and degrees of diagenesis within a very limited area. Most of the samples have dolomite cement, some have later stages of calcite, zeolite or gypsum cement, and few have no evident cement at all. The best conditions for hydrocarbon accumulation and saturation is an uncemented sandstone, as in samples PF-123, PF-124 and PF-141, which have exceedingly high oil saturations of 43.7%, 56.1% and 56.3%, respectively (FIGURE 33). These data can be misleading,

however. For example, FIGURE 33 shows that AS-002 has 24% oil, but this is calculated as the oil-filled fraction of the porosity which is only 4.6%, a very tight sandstone, hence this is a very small amount of oil. FIGURE 34 represents the porosity percentages from the conventional core analysis. Some samples were fractured due to outcrop weathering and preparation/cutting of samples, therefore the actual, in situ porosity was almost certainly less. Calculation of porosity from point-counting measurement can give a much more accurate assessment of initial porosity because fractures suspected as not being original can be skipped and not counted. To better represent the volume of oil per volume of rock, I calculated the "oil in rock volume" (see data chapter) given in FIGURE 35. FIGURE 35 shows clearly the difference in oil between the Altamira Shale and Point Fermin. In general, the Altamira Shale sandstone samples have very low oil volume in rock while the Point Fermin sandstones have high oil volume.

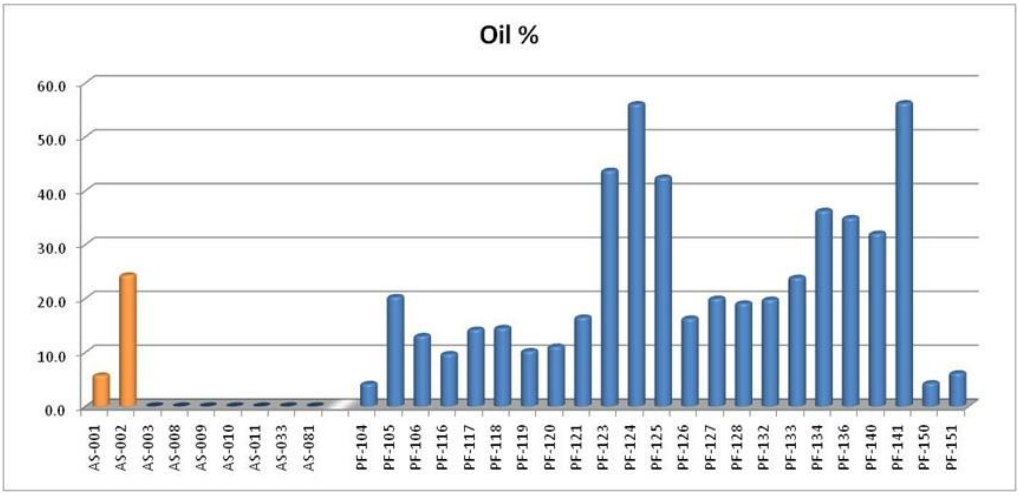

FIGURE 33. Percent oil in pore space by volume. Altamira Shale sandstone samples shown in orange, Point Fermin sandstone samples shown in blue.

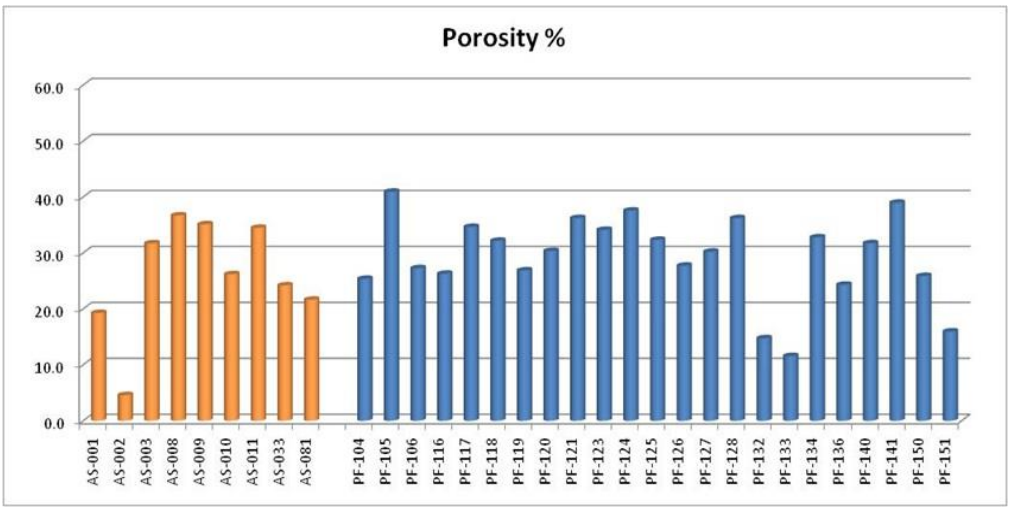

FIGURE 34. Porosity, including both open and fluid-filled pores. Colors as above.

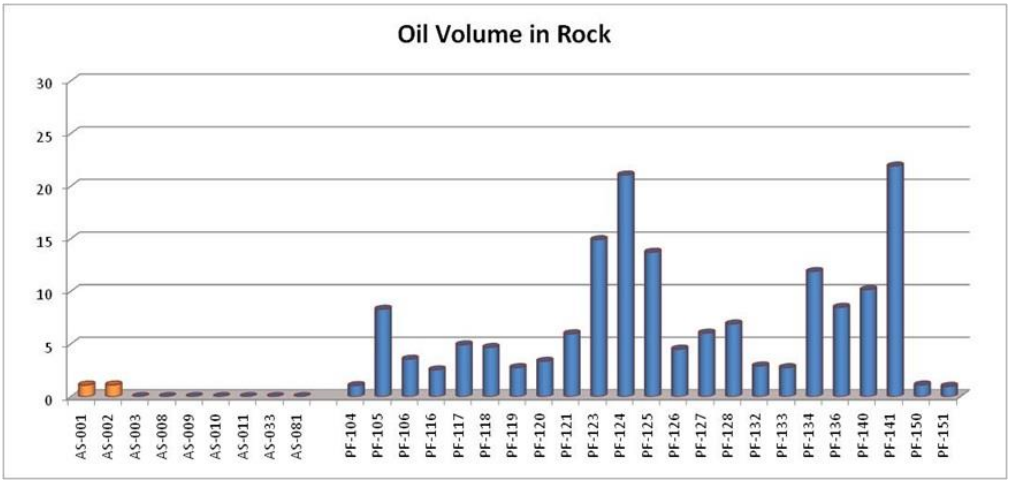

FIGURE 35. Oil volume in rock, calculated from porosity and oil percentage.

Based on conventional core analysis and point counting data, I would suggest that the best cement for maintaining good hydrocarbon reservoir properties is rhombohedral dolomite. This only applies if the rocks have the same degree of cementation and have close range of IGV (Intragranular Volume). The nature of the rhombohedral dolomite cement growth and shape help to preserve the porosity and permeability (FIGURE 36).

Anhedral dolomite cement has lower porosity than the well-shaped rhombohedral dolomite. Calcite cement, another carbonate cement, can be dealt with using acids (FIGURE 37). Zeolite and gypsum cements lower the porosity significantly (FIGURE 38). FIGURE 39 illustrates the different diagenesis types and events that affected the Altamira Shale and Point Fermin. It shows the difference between the two members which in turn affected the heterogeneous oil in rock volume between the two members.

Intragranular Porosity

Many grains show intragranular porosity (Pra). This is especially true for the lithic grains (FIGURE 40). This porosity is most frequently as cracks or partings in schistose metamorphic rock fragments, dissolution in other lithic grains, and minor quartz grains dissolution related to mineral alteration or deformation. Most of the porosity in the Altamira Shale sandstones is intragranular porosity of this type. The grains with intragranular porosity are mainly in samples with cement that occludes most of the pores between the grains. Therefore this intragranular porosity is isolated and ineffective and the samples have low permeability.

IGV

Compaction measured by IGV (Intragranular Volume) shows a difference between the Altamira Shale and the Point Fermin sandstone samples. IGV for the Altamira Shale samples ranged from 17%, to 76%, with an average IGV of 41%. In contrast, the Point Fermin samples IGV ranged from 21% to 41% and averaged 33%.

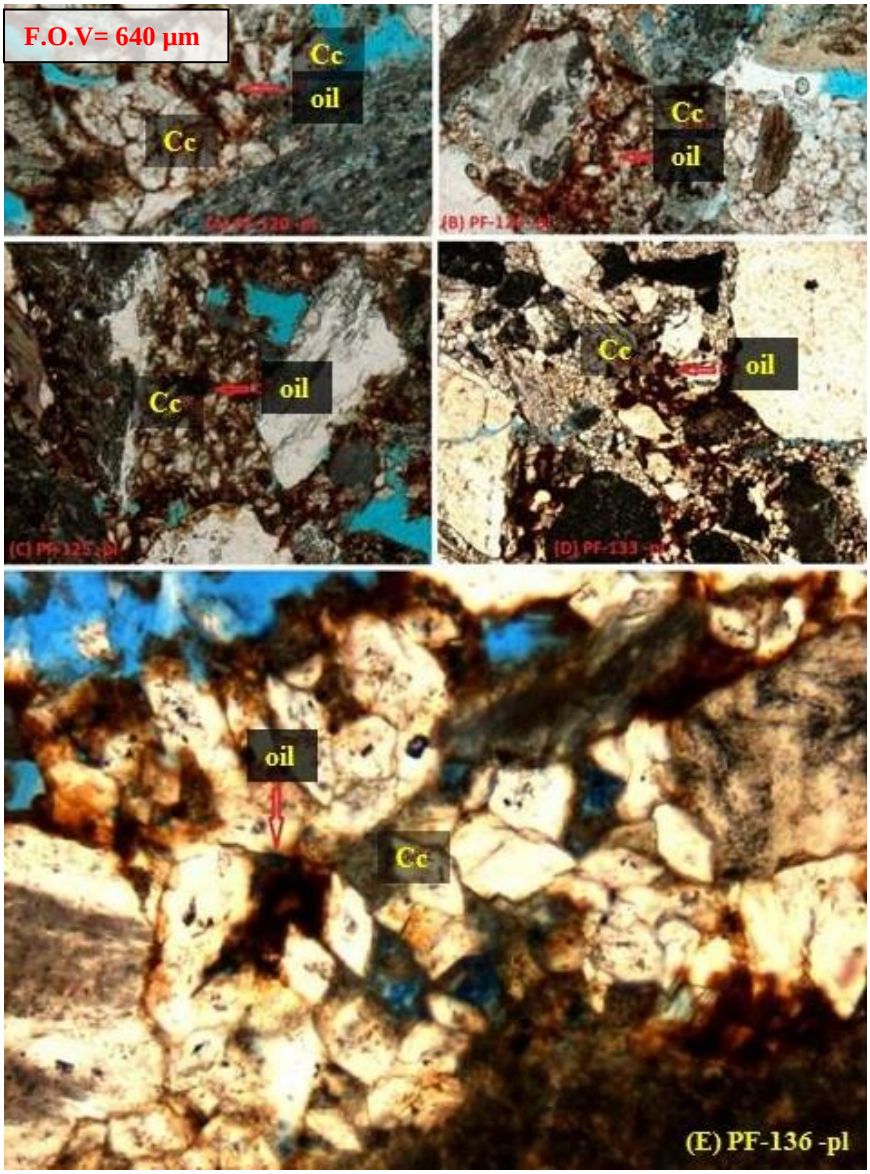

FIGURE 36. Oil in rhombohedral dolomite cement.

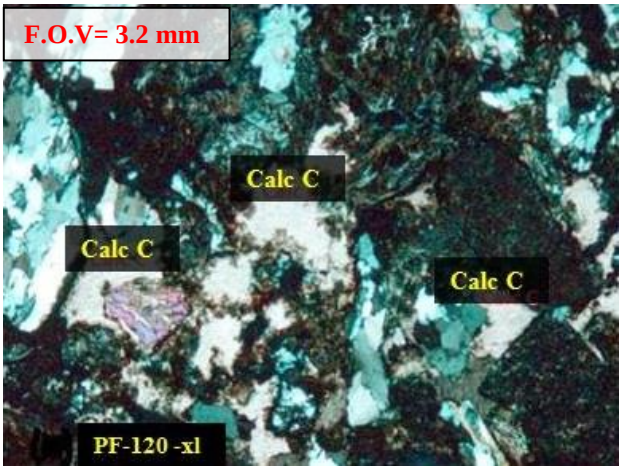

FIGURE 37. Calcite cement.

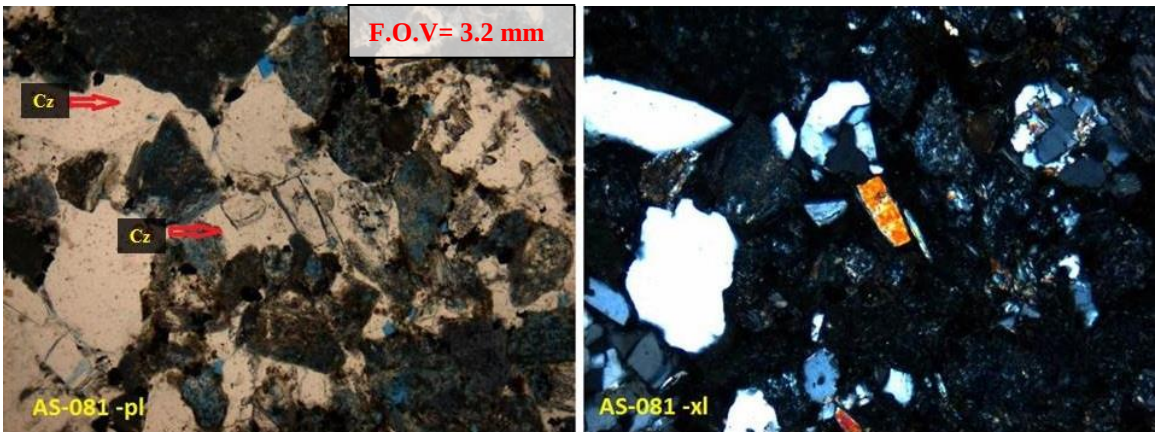

FIGURE 38. Zeolite cement.

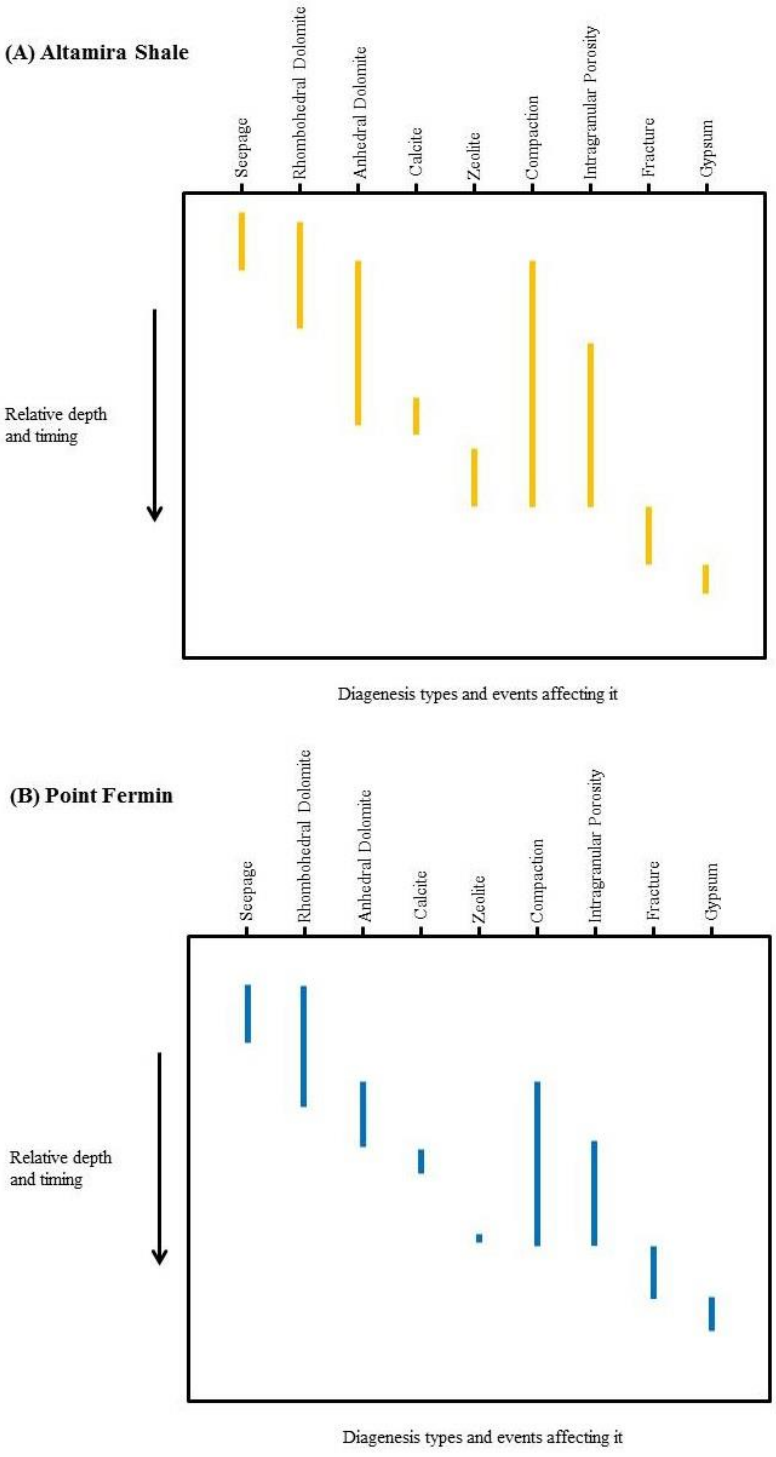

FIGURE 39. Diagenesis diagram for (A) Altamira Shale and (B) Point Fermin.

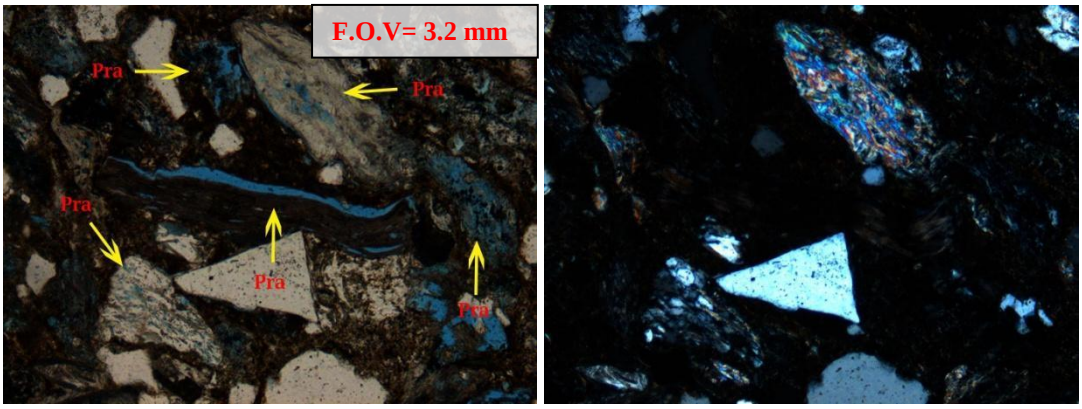

FIGURE 40. AS-008 Intragranular porosity (plain and cross polarized).

Sandstones in the two members differ in IGV by about 10%. These values indicate that the Altamira Shale sandstones are composed of nearly half intergranular volume that consists mainly of cement with little to no porosity. This value is very close to values typical at initial deposition, indicating that the Altamira Shale sandstones were cemented at very shallow burial depths. IGV values are plotted for the Altamira Shale and Point Fermin samples in FIGURE 41.

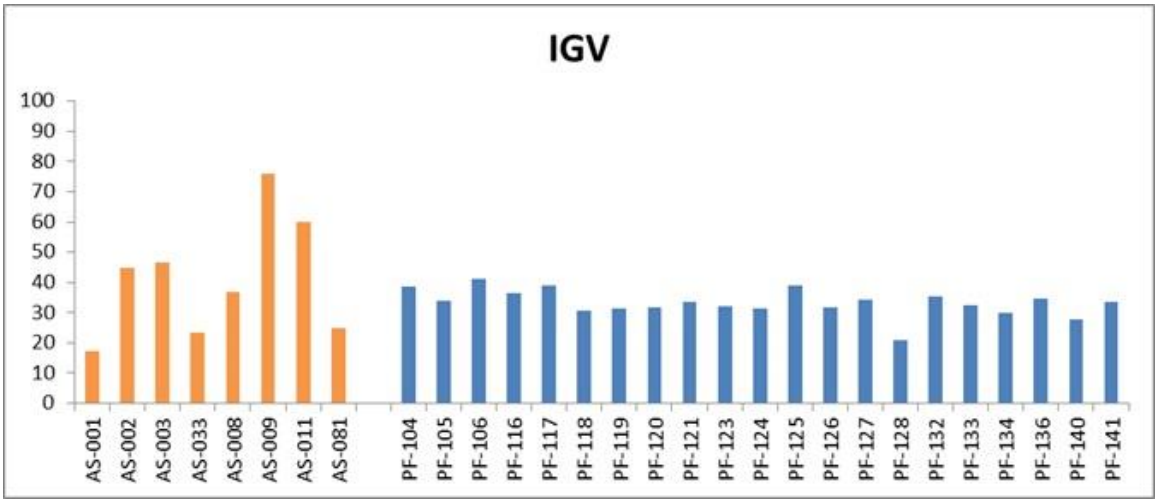

FIGURE 41. Intergranular (IGV) of sandstones from the Altamira Shale and Point Fermin members.

Breaking the IGV down to intergranular porosity (Pin) and cement (C) volumes provide a better understanding of the difference between the two members. The (Pin) percentages for the Altamira Shale samples had minimum value of 0%, maximum value of 4% and average value of 1%. The Point Fermin samples had minimum value of 1%, maximum value of 29%, and average value of 11%. The difference in intergranular porosity between the two members is striking. The Altamira Shale has almost no intergranular porosity, whereas the Point Fermin has good intergranular porosity. A plot

of the intergranular porosity values for all the samples displays this difference between the two members (FIGURE 42).

The total cement (C) percentages for the Altamira Shale sandstones had a minimum value of 17%, maximum of 71%, and average value of 40%. The Point Fermin total cement percentages are minimum value of 4%, maximum value of 34%, and average value of 22%. The difference in cementation is clear. The Altamira Shale has more cement per rock volume than the Point Fermin, with a difference is around 20% on average. This information guides us to understand why oil is not present in the Altamira Shale sandstones, yet is relatively abundant in the Point Fermin samples.

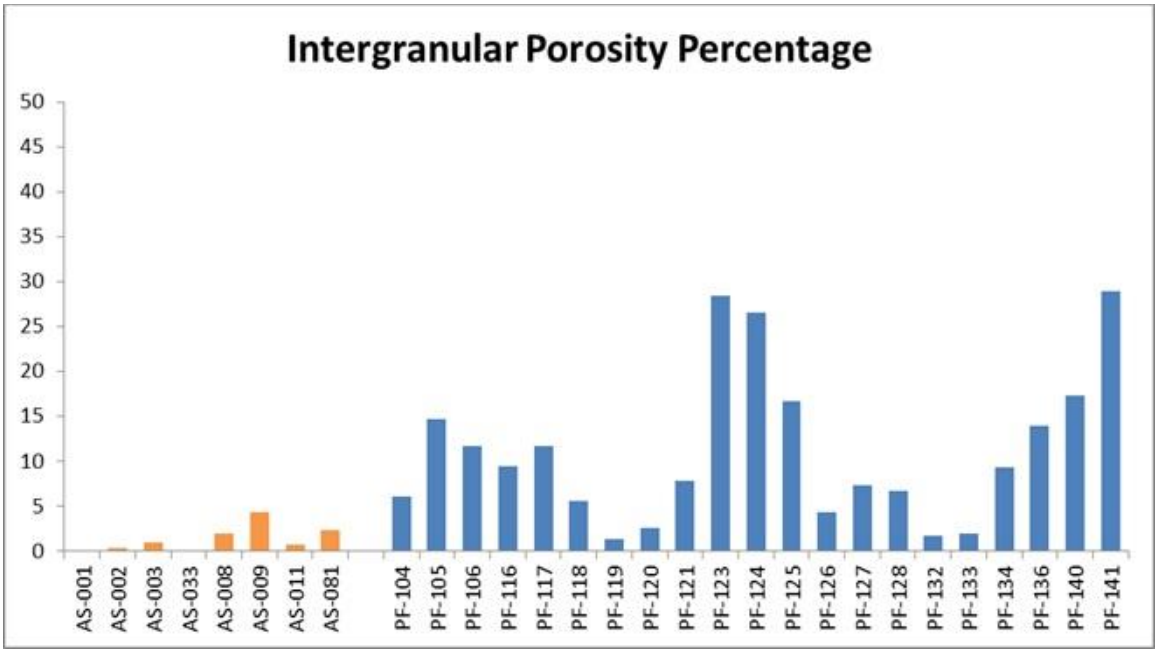

FIGURE 42. Intergranular porosity percentage (Pin).

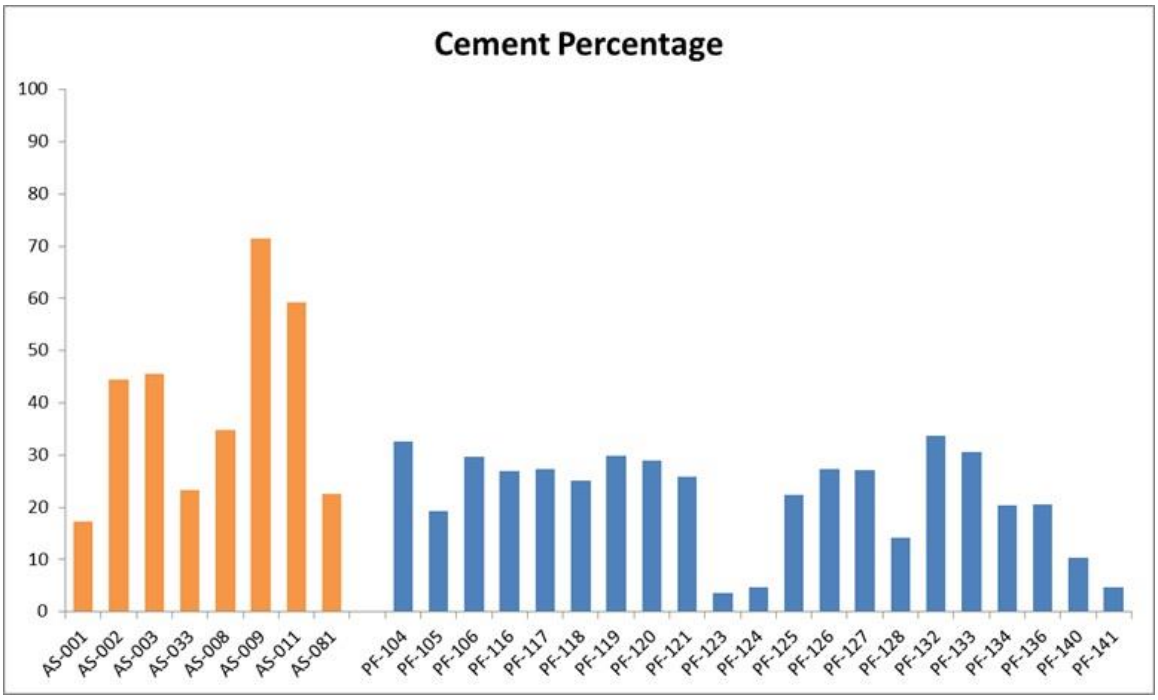

FIGURE 43. Cement Percentage.

The Altamira Shale sandstones were fully cemented by dolomite very shortly after their deposition, at shallow, uncompacted burial depths. This early cementation occluded intergranular porosity and eliminated permeability, preventing later oil impregnation, even into the later-formed intraganular pors in isolated lithic grains. FIGURE 43 indicates the cement percentages difference between the Altamira Shale and Point Fermin sandstones.

The cementation is substantially different between the Altamira Shale samples and the Point Fermin samples. The degree of cementation for the Altamira Shale samples had average of 45%, while the cementation degree in the Point Fermin samples average is 23% (Figure 46). This indicates that the Altamira Shale member underwent earlier cementation prior to significant compaction. The cementation type also plays a part. The

degree of carbonate cementation is different between the Altamira Shale and Point Fermin (FIGURE 43). The Point Fermin samples either have carbonate cement or poor cementation generally. In addition to dolomite and calcite cementation, some of the Altamira Shale samples have significant cementation by zeolites (AS-033 and AS- 081). In contrast, the Point Fermin sandstones samples do not contain later cement of zeolite or gypsum as the main cement. All of these factors indicate a different diagenetic environment or the timing for cementation between the two members.

Grain Size

The sandstones of the Point Fermin member generally have coarser grain size than in the Altamira Shale, although Altamira Shale samples also range from coarse to very coarse sandstone and one sample contains granule-sized grains (Figure 43). In theory, larger grain size relates to increased permeability and the ability to be charged with oil. This could be an additional explanation for the difference in oil saturation between the two units, but it is not supported by the data. Comparing samples of the same size range (very fine-coarse) between the units, there remains a large difference in oil volume in rock. Furthermore, Point Fermin samples with finer grains (PF-124 and PF-141) show somewhat greater oil volume in rock than coarser samples in the same member (see FIGURE 35)**.** This relationship is due to the better sorting of the finer-grained samples. Those observations show that the grain size is not the key factor that causing the dramatic difference in oil volume in rock between the sandstones in Altamira Shale and Point Fermin.

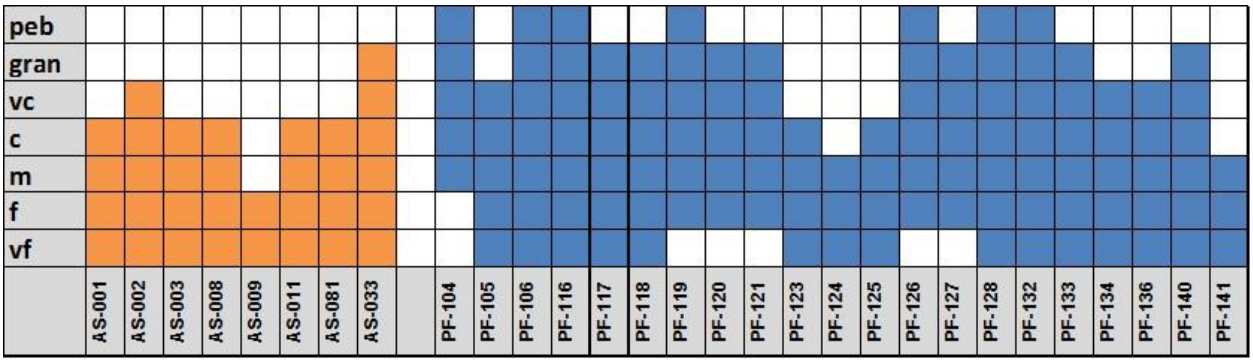

FIGURE 44. Grain size for the Altamira Shale and Point Fermin.

CHAPTER 6

CONCLUSION

This study demonstrated significant differences in hydrocarbon saturation between closely-associated sandstones in the Altamira Shale and Point Fermin members of the Monterey Formation exposed in sea cliffs of the Palos Verdes peninsula, California. Three hypotheses to explain the heterogeneity in oil saturation between the Point Fermin Sandstone and the Altamira Shale sandstone were tested. The first hypothesis that the difference has to do with depositional texture and fabric only can be rejected on the basis that similar texture and fabric sandstones are found in both members and yet they show high difference in oil volume in rock. The second hypothesis that provenances and composition of the sandstones in the two members were different enough to result in different pathways and timing of diagenesis that influenced the potential for hydrocarbon saturation. This hypothesis can also be rejected based on the petrographic data demonstrating that the two members have the same provenance (Catalina Schist) and have the same composition. The third hypothesis that depositional and burial diagenesis environments between the organic-rich shale and coarse-grained submarine channel deposits were different enough to allow for different pathways and timings of diagenesis. This is the preferred hypothesis as shown by substantial differences in intergranular volume, cement volumes, compaction, and types of cement

between the two members. In particular, early cementation of the Altamira Shale sandstones by dolomite impeded saturation by hydrocarbons.

Another important finding is that the dolomite is an organogenic dolomite, likely formed by bacterial activity in the zones of sulfate reduction zone or methanogenesis that would be reached at shallower depths in the organic-rich shale deposits. The first phase of dolomite cementation is characterized by rhombohedral crystals, frequently with hydrocarbon nuclei and intracrystalline porosity. Early presence of hydrocarbons or kerogen might have contributed to localized microenvironments of sulfate reduction for precipitation of the dolomite.

Sandstone beds grade laterally and vertically to fine-grained sandy dolomite in addition to shale. These associations that make Point Fermin a unique place to understand the origin of dolomite. The dolomite beds are observed to have high microfossil content (sponge spicules) that may have contributed to high initial porosities.

Point Fermin presents an excellent location to study and understand the subtlety of stratigraphic traps within unconventional reservoirs because of the demonstrated heterogeneity in petroleum saturation between adjacent sandstone beds associated with dolomite cementation that may be common in organic-rich “shales”.

CHAPTER 7

RECOMMENDATIONS FOR FUTURE RESEARCH

Studying the dolomite interbedded beds within the sandstone submarine channel beds in the Point Fermin would be a valuable study. Usually shale is associated with sandstone channel beds, but that is not the case at Point Fermin. I think would be possible to tie the results with the Deep Sea Drilling Project or Ocean Drilling Program findings (e.g., Wefer et al., 1998). Point Fermin can be a good location to study an outcrop with abundant dolomite in an otherwise organic-rich, but clastic-rich lithofacies.

An additional valuable study would be to investigate why the dolomite crystals have hydrocarbon nuclei? Was the oil inside the dolomite crystals in place before crystal formation or emplaced after growth of the dolomite crystals by some sort of localized dissolution? Finding out if the hydrocarbon inside the crystals have the same chemical or isotopic properties as the intergranular oil in the nearby sandstone will help understanding if some oil has migrated to the formation from another source or at another time.

The architecture of submarine channels has been studied intensively in many publications. The Point Fermin can be another addition in understanding the architecture of submarine channels that can be a good analog for some oil fields. Within the Point Fermin submarine channel, the upper parts of channel stories are well sorted and do not

have cement, in contrast to the majority of sandstone in the Point Fermin. Can this provide information on the timing and heterogeneity of hydrocarbon migration?

Finally, I think studying the microfossils found in the sandy dolomite beds that are interbedded with the sandstone will be a good addition to unravel both the depositional and environmental story as well as the age of the Point Fermin sandstone deposits, which is still poorly constrained.

REFERENCES CITED

REFERENCES CITED

Alan, W. A., et al., 1991, Geochemistry of Los Angeles Basin oil and gas Systems, *in* Biddle, K.T., ed., Active Margin Basins: American Association of Petroleum Geologists Memoir 52, p. 239-259.

Atwater, T., 1970, Implications of plate tectonics for the Cenozoic tectonic evolution of western North America: Geological Society of America Bulletin, v. 81, p. 3513-3536.

Baker, P.A., and Burns, S.J., 1985, The occurrence and formation of dolomite in organic-rich continental margin sediments: America Association of Petroleum Geologists Bulletin, v.69, p. 1917- 1930.

Baker, P.A., and Kastner, M., 1981, Constraints on the formation of sedimentary dolomite: Science, v. 213, p. 215-216.

Barron, J.A., and Isaacs, C.M., 2001, Updated chronostratigraphic framework for the California Miocene, *in* Isaacs, C.M., and Rullkötter, J., ed., The Monterey Formation: from rocks to molecules: New York, Columbia University Press., p. 393-395.

Basinski, P.M., 2013, The golden age of "Shale" exploration: Houston Geological Society Bulletin, v. 55, no. 05, p. 37-43.

Behl, R.J., 1999, Since Bramlette (1946): The Miocene Monterey Formation of California revisited: *in* Moores, et al., ed., Classic Cordilleran Concepts: A View from California: Geological Society of America Special Paper 338, p. 301-313.

Behl, R.J., 2011, Chert spheroids of the Monterey Formation, California (USA): early diagenetic structures of bedded siliceous deposits: Sedimentology, v. 58, p. 325-351.

Behl, R.J., and Garrison, R.E., 1994, The Origin of Chert in the Monterey Formation of California (USA), *in* Iijima, A., ed., Siliceous, Phosphatic and Glauconitic Sediments of the Tertiary and Mesozoic: Proceedings of the 29th International Geological Congress, Part C, p. 101-132.

Behl, R.J., and Morita, S., 2007, The Monterey Formation of the Palos Verdes Hills, California: stratigraphy and diagenetic implications for burial and uplift history: *in* Brown, A.R., et al., ed., Geology and Paleontology of the Palos Verdes Hills, California: A 60th Anniversary Revisit to Commemorate 1946 Publication of U. S. Geological Survey Professional Paper 207: Pacific Section SEPM book 103, p. 51-72.

Blake, G.H., 1991, Review of the Neogene biostratigraphy and stratigraphy of the Los Angeles basin and implications for basin evolution, *in* Biddle, K.T., ed., Active Margin Basins: American Association of Petroleum Geologists Memoir 52, p. 135-184.

Blake, M.C., et al., 1978, Neogene basin formation in relation to plate-tectonic evolution of the San Andreas Fault System, California: American Association of Petroleum Geologists Bulletin, v. 62, p. 344-372.

Bramlette, M. N., 1946, The Monterey Formation of California and the origin of its siliceous rocks: U.S. Geological Survey Professional Paper 212, p.57.

Bryant, M. E., 1982, Geomorphology, neotectonics, and ages of marine terraces, Palos Verdes Peninsula, *in* Guidebook Landslides and Landslide Abatement, Palos Verdes Peninsula, Southern California, Field trip Number 10, pp. 15-25; reprentied: Association of Engineering Geologists, Southern California Section, CA.

Brown, A.R., 2007, Geological overview of the Palos Verdes Peninsula, *in* Brown, A. R., et al., Geology and Paleontology of Palos Verdes Hills, California: A 60th Anniversary Revisit to commemorate the 1946 publication of U.S. Geological Survey Professional Paper 207. p. 5-22.

Californiacoastline.org, 2012: http://www.californiacoastline.org (accessed May 2012)

Cavagna, S., Clari, P., and Martire, L., 1999, The role of bacteria in the formation of cold seep carbonates: geological evidence from Monferrato, Tertiary NW Italy, Sedimentary Geology v. 126, p. 253-270.

Cherven, V.B., and Russell, P.W., 1987, Glaucophane-rich lithic sandstone at Point Fermin, California, *in* Fischer, P.J. ed., Geology of the Palos Verdes Peninsula and San Pedro Bay: Pacific Section, Society of Economic Paleontologists and Mineralogists, Los Angeles, CA, p. 53-56.

Clari, P., Dela Pierre, F., Martire, L., and Cavagna, S., 2009, The Cenozoic CH4-derived carbonates of Monferrato, NW Italy: a solid evidence of fluid circulation in the sedimentary column. Marine Geology v. 265, p. 167-184.

Clarke, D. D., 1987, The structure of the Wilmington Oil Field, *in* Clarke, D. D., and Henderson, C. P., ed., Geologic Field Guide to the Long Beach Area: Pacific Section American Association of Petroleum Geologists, Los Angeles, CA, p. 43-56.

Compton, J.S., 1988, Degree of supersaturation and precipitation of organogenic dolomite. Geology, v. 16, p. 318-321.

Conrad, C.L., 1983, Lithostratigraphy of the Monterey Formation of the Palos Verdes peninsula, Los Angeles county, California [Masters thesis]: Los Angeles, California State University, 96 p.

Conrad, C.L., and Ehlig, P.L., 1983, The Monterey Formation of the Palos Verdes peninsula, California: an example of sedimentation in a tectonically active basin within the California Continental Borderland, *in* Larue, D.K., and Steel, R.J., ed., Cenozoic marine sedimentation, Pacific Margin: SEPM Pacific Section Special Publication, v. 28, p. 103-116.

Core Laboratories, 2012: http://www.corelab.com/rd/petroleumservices/Routine/conventional.aspx (accessed June 2012)

Crouch, J. K., and Suppe, J., 1993, Late Cenozoic tectonic evolution of the Los Angeles basin and inner California Borderland: A model for core complex-like crustal extension: Geological Society of America Bulletin, v. 105, p. 1415-1434.

Deffeyes, K. S., 1959, Zeolites in sedimentary rocks: Journal of Sedimentary Petrology, v. 29, p. 602-609.

Dibblee, T.W., 1999, Geologic map of the Palos Verdes Hills and vicinity, Redondo, Torrance and San Pedro quadrangles, California: Dibblee Geological Foundation, Santa Barbara, Map #DF-70, scale 1:24,000.

Dibblee, T.W., 2000, Geologic History Outline of the Palos Verdes Hills, California, *in* Dibblee, T.W., et al., A Day in the Field with Tom Dibblee in the Palos Verdes Hills, California, p. 16-17.

Dickinson, W.R., 1970, Interpreting detrital modes of graywackeand arkose. Journal of Sedimentary Petrology, v. 40, p. 695-707.

Dickinson, W.R., and Suczek, C.A., 1979, Plate tectonics and sandstone composition: American Association of Petroleum Geologists Bulletin, v. 63, p. 2164- 2182.

Ehlig, P. L., 1982, The Palos Verdes Peninsula; its physiography, land use and geologic setting, in guidebook and volume, in Cooper, J. complier, Landslides and landslide abatement, Palos Verdes Peninsula, Southern California; Field trip Number 10, p. 3-6, host book Association of Engineering Geologists, South California Section, Califonia.

Evans, B.W., 1990, Phase relations of epidote-blueschists: Lithos, v. 25, p. 3-23.

Fayek, M., et al., 2001, In situ stable isotopic evidence for protracted and complex carbonate cementation in a petroleum reservoir, North Coles Levee, San Joaquin Basin, California, U.S.A: Journal of Sediments Research, v. 71, p. 444-458.

Frey, M., de Capitani, C., and Liou, J. G., 1991, A new petrogenetic grid for low grade metabasites: Journal of Metamorphic Geology, v. 9, p. 497-509.

Garzanti, E., and Vezzoli, G., 2003, A classification of metamorphic grains in sands based on their composition and grade: Journal of Sedimentary Research, v. 73, p. 830-837.

Graham, D. J., and Midgley, N. G., 2000, Graphical representation of particle shape using triangular diagrams: an Excel spreadsheet method, Earth Surface Processes and Landforms, v. 25, p. 1473-1477.

Graham, S. A., and Williams, L. A., 1985, Tectonic, depositional, and diagenetic history of Monterey Formation, Miocene, central San Joaquin basin, California: American Association of Petroleum Geologists Bulletin, v. 69, p. 385-411.

Graham, S.A., Ingersoll, R.V., and Dickinson, W.R., 1976, Common provenance for lithic grains in Carboniferous sandstones from Ouachita mountains and Black Warrior basin: Journal of Sedimentary Petrology, v. 46, p. 620-632.

Grove, M., and Bebout, G.E., 1995, Cretaceous tectonic evolution of coastal southern California: Insights from the Catalina Schist: Tectonics, v. 14, p. 1290-1308.

Gunatilaka, A., 1989, Spheroidal dolomites; origin by hydrocarbon seepage? : Sedimentology v.36, p. 701-710.

Harrison, C.P., and Graham, S.A., 1999, Upper Miocene Stevens Sandstone, San Joaquin Basin, California: reinterpretation of a petroliferous, sand-rich, deep-sea depositional system: America Association of Petroleum Geologists Bulletin, v. 83, p. 898-924.

Hewlett, J.S. and Jordan, D.W. 1994, Stratigraphic and combination traps within a seismic sequence framework, Miocene Stevens turbidites, Bakersfield Arch,

California, *in* Weimer, P. et al., ed., Siliciclastic Sequence Stratigraphy: American Association of Petroleum Geologists Memoir 58, p. 135-162.

Holk, G. J., and Brown, A.R., 2007, Preliminary Petrologic Study Of the Catalina Schist in the Palos Verdes Hills, *in* Brown, A. R., et al., 2007, Geology and Paleontology of Palos Verdes Hills, California: A 60th Anniversary Revisit to commemorate the 1946 publication of U.S. Geological Survey Professional Paper 207, p. 41-50.

Ingersoll, R.V., 1999, Three-stage evolution of the Los Angeles basin, southern California: Geology v. 27, p. 593-596.

Ingersoll, R.V., and Suczek, C.A., 1979, Petrology and provenance of Neogene sand from Nicobar and Bengal fans, DSDP sites 211 and 218. Journal of Sedimentary Petrology, v. 49, p. 1217-1229.

Ingersoll, R. V., et al., 1984, The effect of grain size on detrital modes: a test of the Gazzi-Dickinson point-counting method: Journal of Sedimentary Petrology, v. 54, p. 103-116.

Isaacs, C. M., 1980, Diagenesis in the Monterey Formation examined laterally along the coast near Santa Barbara, California [Ph.D. thesis]: Stanford, California, Stanford University.

Kastner, M., et al., 1990, Diagenesis and interstitial-water chemistry at the Peruvian continental margin-major constituents and strontium isotopes, *in* Suess, E., et al., Proceedings of Ocean Drilling Program, Scientific Results, 112: College Station, TX, p. 413-440.

Levandowski, D. W., Kaley, M. E., Silverman, S. R. and Smalley, R. G., 1973, Cementation in Lyons Sandstone and its role in oil accumulation, Denver basin, Colorado: American Association of Petroleum Geologists Bulletin, v. 57, p. 2217-2244.

Luyendyk, B. P., 1991, A model for Neogene crustal rotations, transtension, and transpression in southern California: Geologjeal Society of America Bulletin, v. 103, p. 1528-1536.

Marfil, R., et al., 2010, Dolomite-rich Condensed Sections in Overbank Deposits of Turbidite Channels, the Eocene Hecho Group, south-central Pyrenees, Spain. International Association of Sedimentologists, v. 45, p. 207-230

Mayuga, M. N., 1970, Geology and Development of California's Giant-Wilmington Oil Field: American Association of Petroleum Geologists, Memoir 14, p. 158-184.

Mazzullo, S.J., 2000, Organogenic dolomitization in peritidal to deep-sea sediments: Journal of Sedimentary Research, v. 70, p. 10- 23.

Milliken, K.L., Choh, S. J., and McBride, E.F., 2007, Sandstone Petrology 2.0.1 Multimedia CD-ROM: AAPG/Datapages Discovery Series 10: American Association of Petroleum Geologists, Tulsa, OK.

Morad, S., Al-Ramadan, K., Ketzer, J. M., and De Ros, L. F., 2010, The impact of diagenesis on the heterogeneity of sandstone reservoirs: A review of the role of depositional facies and sequence stratigraphy: American Association of Petroleum Geologists Bulletin, v. 94, p. 1267-1309.

Nielsen, P., Swennen, R., Dickson, J.A.D., Fallick, A.E., and Keppens, E., 1997, Spheroidal dolomites in a Visean karst system-bacterial induced origin: Sedimentology v. 44, p. 177-195.

Noh, J.H., and Boles, J.R., 1993, Origin of zeolite cements in the Miocene sandstones, North Tejon oil fields, California: Journal of Sedimentary Petrology v. 63, p. 248-260.

Norton,T.F., and Otott,G. E., 1996, The stratigraphy of theWilmington oil field: *in* Clarke, D. D., et al., ed., Old oil fields and new life: A visit to the giants of the Los Angeles Basin: American Association of Petroleum Geologists Pacific Section, Guidebook 74, Long Beach.

Obradovich, J., and Naeser, C.W., 1981, Geochronology bearing on the age of the Monterey Formation and siliceous rocks in California, *in* Garrison, R.E., and Douglas, R.G., ed., The Monterey Formation and related siliceous rocks of California: Los Angeles: Pacific Section, Society of Economic Paleontologists and Mineralogists, p. 87-95.

Passey, Q.R., Bohacs, K., Klimentidis, R.E., Esch, W.L., and Sinha, S., 2011, My source rock is now my shale-gas reservoir-characterization of organic-rich rocks: American Association of Petroleum Geologists Annual convention, April 10-13, 2011, Houston, Texas, Abstracts, Search and Discovery Article no. 90124.

Paxton, S.T., Szabo, J.O., Ajdukiewicz, J.M., and Klimentidis, R.E., 2002, Construction of an intergranular volume compaction curve for evaluating and predicting compaction and porosity loss in rigid-grain sandstone reservoirs: American Association of Petroleum Geologists Bulletin, v. 86, p. 2047-2067.

Pierce, J.W., and William, G.M., 1967, Dolomite from the continental slope of Southern California: Journal of Sedimentary Research, v. 37, p. 963-966.

Pisciotto, K. A., 1981, Diagenetic trends in the siliceous facies of the Monterey Shale in the Santa Maria region, California: Sedimentology, v. 28, p. 547-571.

Pisciotto, K. A., and Garrison, R. E., 1981, Lithofacies and Depositional Environments of the Monterey Formation, California, *in* Garrison, R. E., and Douglas, R. G., ed., The Monterey Formation and related siliceous rocks of California: Los Angeles, Pacific Section, Society of Economic Paleontologists and Mineralogists, p. 97-122.

Platt, J.P., 1975, Metamorphism and deformational processes in the Franciscan Complex, California: Some insights from the Catalina Schist terrane: Geological Society of America Bulletin, v. 86, p. 1337-1347.

Redin, T., 1991, Oil and gas production from submarine fans of the Los Angeles basin: a guide to migration history, *in* Biddle, K.T. ed., Active Margin Basins. American Association of Petroleum Geologists Memoir 52, p. 239-259

Roehl, P. O., 1981, Dilation brecciation-proposed mechanism of fracturing, petroleum expulsion, and dolomitization in Monterey Formation, California, *in* Garrison, R. E., and Douglas, R. G., ed., The Monterey Formation and related siliceous rocks of California: Los Angeles, Pacific Section, Society of Economic Paleontologists and Mineralogists, p. 285-315.

Rowell, H.C., 1982, Chronostratigraphy of the Monterey Formation of the Palos Verdes Hills, in Cooper, J.D. compiler, Landslides and landslide abatement, Palos Verdes peninsula, southern California: Geological Society of America Cordilleran Section field trip no. 10, volume and guidebook, p.7-13.

Rumelhart, P.E., and Ingersoll, R.V., 1997, Provenance of the upper Miocene Modelo Formation and subsidence analysis of the Los Angeles Basin, southern California; implications for paleotectonic and paleogeographic reconstructions: Geological Society of America Bulletin v. 109, p. 885-899.

Russell, P.W., 1987, Point Fermin submarine fan: A small late middle Miocene age fan within the Monterey Formation. In: Fischer, P.J., ed., Geology of the Palos Verdes Peninsula and San Pedro Bay: Pacific Section, Society of Economic Paleontologists and Mineralogists, Los Angeles, CA, p. 31-46.

Schwartz, D.E., and Colburn, I.P., 1987, Late tertiary to recent chronology of the Los Angeles Basin, Southern California. In: Fischer, P.J. ed., Geology of the Palos Verdes Peninsula and San Pedro Bay: Pacific Section, Society of Economic Paleontologists and Mineralogists, Los Angeles, CA, pp. 5-16.

Schwiebert, J.F., and Francis, R.D., 2007, Tectonic Origin of the Cabrillo Fault, Palos Verdes Peninsula and Adjacent San Pedro Shelf, *in* Brown, A. R., et al., Geology and Paleontology of Palos Verdes Hills, California: A 60th Anniversary Revisit to

commemorate the 1946 publication of U.S. Geological Survey Professional Paper 207, p. 223-231.

Shimmield, G.B., and Price, N.B., 1984, Recent dolomite formation in hemipelagic sediments off Baja California, Mexico, *in* Garrison, R.E., et al., ed., Dolomites in the Monterey Formation and Other Organic-rich Units: Special Publication, Society of Economic Paleontologists and Mineralogists, v. 41, p. 5-18.

Slatt, R. M., 1986, Exploration models for submarine slope sandstone: Gulf Coast Association of Geological Societies Transactions, v. 36, p. 295-304.

Sloan, J. R.., 1987, Age and Paleooceanography of the Point Fermin fan complex, *in* Fischer, P.J. ed., Geology of the Palos Verdes Peninsula and San Pedro Bay: Pacific Section, Society of Economic Paleontologists and Mineralogists, Los Angeles, CA, p. 47-52.

Smith, R. E., 1969, Petrography-porosity relations in carbonate-quartz system, Gatesburg formation, late Cambrian, Pennsylvania: American Association of Petroleum Geologists Bulletin, v. 53, p. 261-278.

Spotts, J. H., 1964, Grain orientation and imbrication in Miocene turbidity current sandstones, California: Journal of Sedimentary Petrology, v. 34, p. 229-253

Spotts, J. H, and Silverman, S. R, 1966, Organic dolomite from Point Fermin, California: The American Mineralogist, v. 51, p. 1144-1155.

Suess, E., et al., 1988, Proceedings, Ocean Drilling Program, Initial Reports, 112: College Station, TX.

Suttner, L.J., and Dutta, P.K., 1986, Alluvial sandstone composition and paleoclimate, I. Framework mineralogy: Journal of Sedimentology Petrology, v. 56, p. 329-345.

Taylor, J.C.M., 1978, Control of diagenesis by depositional environment within a fluvial sandstone sequence in the northern North Sea Basin; Journal of the Geological Society of London, v. 135, p. 83-91.

Truex, J. N., 1972, Fractured shale and basement reservoir, Long Beach Unit, California: American Association of Petroleum Geologists Bulletin, v. 56, no. 10, p. 1931-1938.

Tucker, M.E., 2001, Sedimentary Petrology: An Introduction to the Origin of Sedimentary Rocks, 3rd ed., Blackwell Science, Oxford, p. 42-55.

Turcotte, D. L., and D.C. McAdoo, 1979, Thermal subsidence and petroleum generation in the southwestern block of the Los Angeles Basin, California: Journal of Geophysical Research, v. 84, p. 3460-3464.

U.S. Energy Information Administration, 2013, Annual energy outlook, early release 2013: DOE/EIA- 03383ER, p. 1-2.

Waldschmidt, W. A., 1941, Cementing Materials in Sandstones and Their Probable Influence on Migration and Accumulation of Oil and Gas: American Association of Petroleum Geologists, v. 25, no. 10, p. 1859-1879.

Warren, J., 2000, Dolomite: occurrence, evolution and economically important associations: Earth-Science Reviews, v. 52, p. 1-81.

Wefer, G., Berger, W. H., and Richter, C., 1998, Facies patterns and authigenic minerals of upwelling deposits off Southwest Africa: Proceedings of the Ocean Drilling Program, Initial Report, p. 487-504.

Woodring, W. P., Bramlette, M. N., and Kew, W. S., 1946, Geology and paleontology of Palos Verdes Hills, California: USGS Professional Paper 207, 145 p.

Wright, D.T., and Wacey, D., 2005, Precipitation of dolomite using sulphate-reducing bacteria from the Coorong Region, South Australia: significance and implications: Sedimentology, v. 52, p. 987-1008.

Wright, T.L., 1991, Structural geology and tectonic evolution of the Los Angeles basin, California, *in* K.T. Biddle, ed., Active margin basins: American Association of Petroleum Geologists, Memoir 52, p. 35-130.

Yerkes, R. F., McCulloh, T. H., Schoellhamer, J. E., and Vedder J. G., 1965, Geology of the Los Angeles Basin California-An Introduction: U. S. Geological Survey professional Paper 420-A, 57 p.

Zenger, D.H., Dunham, J.B., and Ethington, R.L., 1980, Concepts and models of dolomitization, Special Publication 28: Society of Economic Paleontologists and Mineralogists, 320 pp.